

DiFaReli++: Diffusion Face Relighting with Consistent Cast Shadows

Puntawat Ponglertnapakorn, Nontawat Tritrong, and Supasorn Suwajanakorn*



Fig. 1: Our method addresses one of the most challenging relighting scenarios where input images contain strong highlights and cast shadows. It effectively removes these effects and generates convincing shading and temporally consistent new shadows—all in a single network pass, given pre-processed input data. It also works across varying head poses, identities, and facial makeup.

Abstract—We introduce a novel approach to single-view face relighting in the wild, addressing challenges such as global illumination and cast shadows. A common scheme in recent methods involves intrinsically decomposing an input image into 3D shape, albedo, and lighting, then recomposing it with the target lighting. However, estimating these components is error-prone and requires many training examples with ground-truth lighting to generalize well. Our work bypasses the need for accurate intrinsic estimation and can be trained solely on 2D images without any light stage data, relit pairs, multi-view images, or lighting ground truth. Our key idea is to leverage a conditional diffusion implicit model (DDIM) for decoding a disentangled light encoding along with other encodings related to 3D shape and facial identity inferred from off-the-shelf estimators. We propose a novel conditioning technique that simplifies modeling the complex interaction between light and geometry. It uses a rendered shading reference along with a shadow map, inferred using a simple and effective technique, to spatially modulate the DDIM. Moreover, we propose a single-shot relighting framework that requires just one network pass, given pre-processed data, and even outperforms the teacher model across all metrics. Our method realistically relights in-the-wild images with temporally consistent cast shadows under varying lighting conditions. We achieve state-of-the-art performance on the standard benchmark Multi-PIE and rank highest in user studies. Please visit our page: <https://diffusion-face-relighting-pp.github.io>

Index Terms—Face relighting, Diffusion models, Conditional diffusion implicit models, Shadow manipulation, Image editing

I. INTRODUCTION

RELIGHTING face images under various lighting conditions is a key aspect of portrait photography and artistic image editing. It involves adjusting facial shading to new lighting while accounting for global illumination and subsurface scattering effects that produce soft lighting transitions and a realistic skin appearance, as well as self-occlusion for hard cast shadows. These capabilities enable applications such as digital characters that adapt to virtual lighting, cinematic effects for filmmakers, and virtual try-on. However, achieving such realism and control in single-view face relighting is challenging, as it requires modeling light interactions with facial geometry and materials from just one image.

Earlier work [5], [72], [35], [89], [75] often assumes Lambertian surfaces and simplified lighting models, which struggle to capture complex light interactions, such as indirect lighting or cast shadows. Using multi-view, multi-illumination data from a light stage or a simulation, [48], [29], [51], [34], [96], [46] proposed relighting pipelines that predict surface normals, albedo, and a set of diffuse and specular maps with neural networks given a target HDR map. Recent methods explicitly model cast shadows through shadow maps, either by predicting them using a neural network [29], [48] or by rendering with physical ray tracing with estimated geometry [28].

Despite progress, state-of-the-art methods still struggle with photorealistic relighting in challenging in-the-wild scenarios,

[†]P. Ponglertnapakorn, N. Tritrong, and S. Suwajanakorn are with the School of Information Science and Technology, Vidyasirimedhi Institute of Science and Technology, Thailand. E-mail: {puntawat.p_s19, nontawat.t_s19, supasorn.s}@vistec.ac.th

^{*}Published in IEEE Transactions on Pattern Analysis and Machine Intelligence (TPAMI), vol. 48, pp. 5068-5082, May 2026. DOI: 10.1109/TPAMI.2025.3648667

*Corresponding author

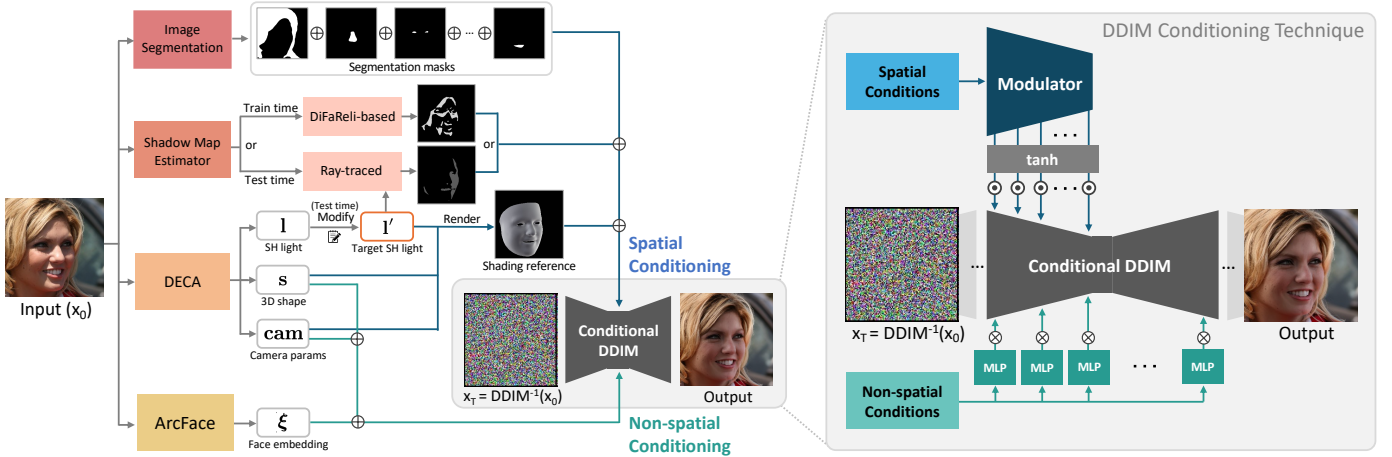


Fig. 2: **Overview of DiFaReli++.** We use off-the-shelf estimators to derive various encodings from the input image: segmentation masks, shadow map, (light, shape, camera) parameters, and face embedding. These encodings are then fed into a conditional DDIM via “spatial” and “non-spatial” conditioning techniques. For spatial conditioning, a shading reference, shadow map, and segmentation masks are concatenated and fed into the Modulator to produce spatial modulation weights for the first half of the DDIM. Meanwhile, the 3D shape, camera, and face embedding are concatenated and processed by a set of MLPs, which modulate the DDIM using a modified version of adaptive group normalization (AdaGN). For DiFaReli, please see Figure 18.

often failing to remove or add strong highlights and cast shadows realistically, leading to residual artifacts (Figure 6) or less convincing results.

These issues arise from a common strategy in these pipelines: decomposing the face into surface normals, albedo, and lighting parameters to render the relit output. This process heavily depends on the accuracy of these estimated components, which is challenging to achieve in real-world scenarios and directly impacts the realism of the final result. Additionally, geometry estimation for other areas like hair and ears is extremely difficult and often omitted from relighting pipelines, leading to unrealistic composites (Figure 6 and 7).

This paper introduces an alternative approach that does not rely on accurate intrinsic face decomposition and is trained solely on 2D images—without 3D scans, multi-view images, relit pairs, or lighting ground truth—once given a few off-the-shelf estimators. Our general idea is simple: we first encode the input image into a feature vector that disentangles lighting from other information about the input image. Then, we modify the light encoding and decode it. The challenge lies in disentangling lighting so that only shading changes while shape and identity remain intact. Our key idea is to leverage a conditional diffusion implicit model [78] with a novel conditioning technique to learn complex light interactions implicitly via the generative model trained on real-world 2D face data.

Our method builds on mechanisms from Denoising Diffusion Implicit Models (DDIM) [78] and Diffusion Autoencoders (DiffAE) [56]. Leveraging DDIM’s deterministic reversal, DiffAE encodes an image into a meaningful semantic code disentangled from other information. By modifying and decoding the semantic code, DiffAE can manipulate attributes in real images. Relighting can be viewed as manipulating the “light” attribute. But unlike DiffAE, which discovers semantic attributes automatically and encodes them in a *latent* code, our method requires an explicit and interpretable light encoding that facilitates lighting manipulation by the user.

To solve this without lighting ground truth, we use an off-the-shelf estimator, DECA [16], to encode lighting information as spherical harmonic (SH) coefficients and employ a conditional DDIM to decode and disentangle the light information in the process. Unlike prior work, we do not use SH lighting to directly render the output, which is limited in capturing complex illumination. Instead, we use it to condition a generative process that learns complex shading priors to reproduce real-world 2D face images. To help preserve identity during relighting, we also condition the DDIM on attributes such as face shape and Arcface embeddings [10].

Another key component is our conditioning technique for DDIM. Instead of using SH lighting as a global conditioning vector as in DiffAE, we render a shading reference via the known SH equation and feed it to a *Modulator* network, which computes layer-wise spatial modulation weights for DDIM. This scheme helps preserve spatial information in the shading reference and provides an easy-to-learn signal, since its pixel intensities correlate directly with the output RGB values. Note that a similar spatial modulation idea, though not designed for relighting, was proposed in ControlNet [99], released concurrently with our conference version DiFaReli [54].

In DiFaReli, cast shadows are controlled by a single scalar for “intensity,” allowing adjustment of hard shadows (Fig. 8). However, these shadows may not always appear physically plausible as target lighting changes. For instance, as the sun moves overhead, the shadows cast by the nose should sweep naturally across the face rather than simply fading in and out, as DiFaReli sometimes produces.

Our extended DiFaReli++ addresses this by augmenting the shadow conditioning signal with information capturing the exact shape of cast shadows and using it to condition our DDIM. Unlike prior work [29], [28], which estimate shadow maps with error-prone lighting and geometry estimates [28], often causing DDIM to disregard the conditioning signal entirely, we propose a simple yet effective method: use DiFaReli to

generate stronger and weaker cast-shadow versions of the input image, then compute their pixel difference (Fig. 3). At test time, we use ray tracing solely to generate a new conditioning shadow map, which guides the network in synthesizing the final composite (Figure 9).

Additionally, we expand DeFaReli’s relightable area to include clothing and hats by relaxing our previous hard constraints. Specifically, we use segmentation masks inferred from an off-the-shelf segmentation network [97] instead of raw background pixels to condition the DDIM, enabling relighting while preserving scene and facial structures.

As our framework is based on diffusion models, it is slow due to the multiple steps required for image denoising and inversion. To address this, we propose a single-shot framework that includes dataset generation and training of a single-shot relighting network. Using the same architecture as DiFaReli++, the single-shot network can be trained with a simple supervised L2 loss, without requiring complicated distillation losses or training [70], [95], [79].

We conduct qualitative and quantitative evaluations, along with user studies. Our method achieves state-of-the-art performance on the standard Multi-PIE benchmark [21] and receives top ratings across all scenarios. Our method produces highly plausible and photorealistic results with consistent cast shadows. Compared to recent work, our method better preserves details (Figure 19) and handles inputs with cast shadows more effectively (Figure 20). Surprisingly, our distilled single-shot framework even outperforms the teacher model across all visual metrics and achieves a 1,000× speedup once the input has been pre-processed (Figures 11 and 12).

To summarize, this paper introduces two key contributions, which are presented in its conference version [54]:

- A state-of-the-art face relighting framework based on a conditional DDIM that produces photorealistic shading without requiring accurate intrinsic decomposition or 3D and lighting ground truth.
- A novel conditioning technique that converts a shading reference rendered from the estimated light and shape parameters into layer-wise spatial modulation weights.

Extending the conference version, this paper introduces DiFaReli++ with the following additions:

- *Relighting with consistent cast shadows (Section IV-A)*: We enhance cast shadow consistency and realism under dynamic lighting by utilizing a conditioning shadow map inferred using a novel technique based on DiFaReli.
- *Expanding relightable area (Section IV-B)*: We replace raw-pixel background conditioning in DiFaReli with segmentation masks, expanding relightable regions to non-facial parts like clothing and hats.
- *A single-shot relighting framework (Section IV-C)*: A simple distillation technique that improves quality over the diffusion-based DiFaReli++ and significantly speeds up inference given all pre-processed data.
- *User studies and concurrent work comparison (Section V-C, V-A, V-D and VI-A)*: We conducted additional experiments, user studies to evaluate relighting quality for facial / non-facial parts and cast shadow consistency, and

comparisons with concurrent work (DiffusionRig [13], IC-Light [100], HoloRelighting [46], SwitchLight [34], Neural Gaffer [31], and Guo et al. [22]).

II. RELATED WORK

A common approach to face relighting [5], [85], [35], [72], [89], [75] is to decompose an input image into intrinsic components (e.g., lighting, albedo, surface normals) and recombine it back with modified light-related components. Decomposition can be done by regularized optimization [5], morphable model fitting [6], [89], or neural prediction [72], [35], [85], [48], [90], [51], [75], [52], [13], [18], [61], [34], [22]. Most earlier methods [5], [72], [35], [89], [75] assume Lambertian surfaces, simplified lighting (e.g., second-order spherical harmonics), and a physical image formation, making them unable to handle real-world effects such as specular highlights or cast shadows.

Instead of physical decomposition, some methods [105], [81] use encoder-decoder networks with a latent lighting representation. Zhou et al. [105] constrain this code to predict SH lighting and train another regressor that maps the SH lighting of a reference image to a latent code for relighting. Sun et al. [81] use low-resolution illumination maps, obtained from a light stage, e.g., [92], instead of the SH lighting. In principle, these models can learn hard shadows and specularities with enough data, but in practice they struggle due to limited light stage data [81] or limited variations in synthetic datasets [105].

Handling non-diffuse components. Nestmeyer et al. [48] use a two-stage framework, predicting non-diffuse components as residuals over a diffuse rendering and cast shadows via a visibility map. Wang et al. [90] instead use intrinsic decomposition to learn shadow and specular maps from a large-scale relighting dataset. Pandey et al. [51] predict specular maps with varying Phong exponents from estimated normals and an HDR environment map. Combined with diffuse and albedo maps, these are used in a UNet to generate a relit image. Yeh et al. [96] and Kim et al. [34] follow a pipeline similar to [51] with different modifications: Yeh et al. use synthetic light stage data from 3D scans and an albedo refinement step to reduce the synthetic-real gap, while Kim et al. adopt the Cook-Torrance model with an additional pre-training stage. Hou et al. [29] fit a morphable model and use ray tracing to compute a shadow map for predicting pixel luminance ratios in relighting. Later, Hou et al. [28] predicted a shadow mask from estimated depth via ray tracing and rendered relit images using network-predicted albedo and shading maps.

While these methods [48], [29], [28] produce promising non-diffuse effects, their reliance on physical image formation makes them sensitive to geometry errors. Thus, some [29], [28] can only relight the face, not ears or hair, and still fail on in-the-wild cast shadows (Figure 6 and 9). Neural rendering methods [90], [51], [34] handle estimation errors better but often lose high-frequency details, even when predicted by a UNet [90]. Many methods [51], [34] rely on high-quality, proprietary light stage data for training, but capturing large, diverse datasets remains challenging. Synthetic light stage data [96] helps bridge the domain gap but depends on 3D face scans, which are harder to obtain than 2D images.

Fine-tuning strategies [61], [34] further improve results, yet dependence on light stage data remains unavoidable. Other related studies [24], [69] focus on subject-specific relighting using 3D Gaussian splatting but are unsuitable for in-the-wild relighting, as they require diffuse inputs [24] or multiview video data [69], which are not readily obtainable from in-the-wild scenarios. Another research direction [98], [31] targets object relighting, but these methods typically do not generalize well to faces and require multi-view light-stage data for fine-tuning, which lacks the quality and diversity of object datasets.

Style transfer-based methods. Some approaches [37], [43], [73] adapt style transfer to relighting by transferring lighting and shading styles between images, though they were not originally designed for face relighting. However, these style-based methods capture information beyond lighting and fail to produce accurate relit results. Shu et al. [74] address relighting with spatially varying color histogram matching based on face geometry, formulated as a mass transport problem. Yet, it does not model self-occlusion for cast shadows and is sensitive to occlusion from hair or accessories. Other methods [61], [100], [87], [33] perform background-based harmonization, transferring lighting from background to subject. Since they require a background and focus on composites, they are not directly comparable to our method.

GAN-based methods. A few techniques use GANs [20] for relighting [83], [44], [60]. Ranjan et al. [60] condition a tri-plane generator in EG3D [7] on lighting estimates from DECA [16] to learn a disentangled 3D generative model with lighting and pose control. However, they do not demonstrate relighting results for real images. Mei et al. [46] also build on EG3D and implicitly model lighting effects instead of using explicit reflectance models, improving upon Ranjan et al. [60] and successfully handling real images. Tewari et al. [83] build on StyleRig [84], which provides semantic control of StyleGAN [32] by mapping morphable model parameters and a StyleGAN latent code to a new code representing target parameters. While StyleRig originally worked only on synthetic images, they extend it to real images by optimizing a latent code to reconstruct the input and then manipulating the lighting through StyleRig. Similarly, Mallikarjun et al. [44] map target illumination and a pSp-predicted StyleGAN code [62] to a new code for relighting. However, their imperfect GAN inversion often alters identity and facial details. New GAN inversion methods [15], [63], [94] are promising, but only [46] show real-image relighting. However, it requires fine-tuning EG3D for each input image. In contrast, our method leverages DDIM’s near-perfect inversion to preserve details without person-specific fine-tuning.

Acceleration of diffusion sampling. Training-based methods [91], [3], [70], [79], [95] address this at the cost of additional training, often via distillation. Recent approaches such as UFOGen [95], Consistency Models [79], and Adversarial Diffusion Distillation [70] achieve single-step sampling but require complex losses (e.g., adversarial) and still lag behind teacher performance. Training-free methods [41], [42], [104] use fast solvers applicable to any pretrained diffusion model, reducing sampling to 5–10 steps but still short of single-shot inference, with a notable quality–speed trade-off.

This paper demonstrates that training a network on relit pairs from pretrained DiFaReli++ with simple L2 loss enables single-step generation with quality surpassing DiFaReli++.

III. APPROACH

Given an input face image, we aim to relight it under a target lighting condition, described by SH coefficients and a representation of cast shadows. In DiFaReli++, we represent cast shadows with a shadow map capturing both intensity and shape, unlike DiFaReli, which uses only a scalar for intensity.

To explain our method, we first cover the relevant background on DDIM [78] and a key finding from DiffAE [56] in Section III-A, which demonstrates how a conditional DDIM can perform attribute manipulation on real images by functioning as both a decoder and a ‘stochastic’ encoder. In Sections III-B to III-G, we review the core concepts of DiFaReli, including its conditioning technique, as well as the details of its training and relighting processes. Finally, in Section IV, we introduce DiFaReli++, an extension of DiFaReli that incorporates shadow map conditioning, non-facial part relighting, and a single-shot relighting framework.

A. Background: Conditional DDIM & DiffAE

Our method relies on a conditional Denoising Diffusion Implicit Model (DDIM) [78], which is a variant of diffusion models [77], [25], [80]. Unlike standard diffusion models, DDIM uses a non-Markovian inference process that relies on the conditional distribution $q(\mathbf{x}_{t-1} | \mathbf{x}_t, \mathbf{x}_0)$ that is conditioned on \mathbf{x}_0 (the original image) in addition to \mathbf{x}_t . One important implication is that the generative process can be made deterministic, allowing us to deterministically map $\mathbf{x}_T \sim \mathcal{N}(\mathbf{0}, \mathbf{I})$ to \mathbf{x}_0 and vice versa. Here the mapping from \mathbf{x}_0 to \mathbf{x}_T can be viewed as the encoding of an input image \mathbf{x}_0 to a latent variable \mathbf{x}_T .

Diffusion Autoencoders (DiffAE) [56] show that such image encoding yields \mathbf{x}_T that contains little semantic information about the input image \mathbf{x}_0 and propose to condition the DDIM also on a learnable latent variable \mathbf{z} predicted from a separate image encoder. By jointly training the image encoder and the DDIM, the encoded \mathbf{z} now captures meaningful semantics, while the encoded \mathbf{x}_T , inferred by reversing the deterministic generative process of the DDIM, captures the rest of the information not encoded in \mathbf{z} , such as stochastic variations. The resulting latent code $(\mathbf{z}, \mathbf{x}_T)$ can also be decoded back to the input image near-perfectly using the same conditional DDIM. By modifying the semantic latent \mathbf{z} and decoding the new $(\mathbf{z}', \mathbf{x}_T)$, DiffAE can manipulate semantic attributes of a real input image—a capability that inspires our work.

B. DiFaReli: Method overview

The general idea of DiFaReli is to encode the input image into a feature vector that disentangles the light information from other information about the input image. Then, the relit image is produced by modifying the light encoding in the feature vector and decoding the resulting vector with a conditional DDIM (Figure 2). This process is similar to how

DiffAE performs attribute manipulation; however, our task requires well-disentangled and interpretable light encoding that facilitates lighting manipulation by the user.

To solve this, we use off-the-shelf estimators to encode an input image into light, shape, and camera encodings, as well as a face embedding, a shadow scalar, and a background image (Section III-C). Then, these encodings are used to condition our DDIM decoder (Section III-D) with a novel conditioning technique (Section III-E). For training, we use a standard diffusion objective to reconstruct training images (Section III-F). To relight, we reverse the generative process of the DDIM conditioned on the input’s encodings to obtain \mathbf{x}_T , modify the light encoding, and decode \mathbf{x}_T using the modified encodings (Section III-G).

C. DiFaReli: Encoding

The goal of this step is to encode the input face image $I \in \mathbb{R}^{H \times W \times 3}$ into a feature vector:

$$\mathbf{f} = (\mathbf{l}, \mathbf{s}, \mathbf{cam}, \xi, c, \mathbf{bg}), \quad (1)$$

where $\mathbf{l} \in \mathbb{R}^{9 \times 3}$ represents 2nd-order spherical harmonic lighting coefficients, $\mathbf{s} \in \mathbb{R}^{|\mathbf{s}|}$ represents parameterized face shape, $\mathbf{cam} \in \mathbb{R}^{1+2}$ represents orthographic camera parameters, $\xi \in \mathbb{R}^{512}$ is a deep feature embedding based on ArcFace [10], c is a scalar that indicates the intensity of visible cast shadows, and $\mathbf{bg} \in \mathbb{R}^{H \times W \times 3}$ contains the background pixels with the face, hair, neck masked out. These variables will be inferred using off-the-shelf or pretrained estimators.

Light, shape, & camera encodings ($\mathbf{l}, \mathbf{s}, \mathbf{cam}$). We use DECA [16], an off-the-shelf single-view 3D face reconstruction method that predicts the 3D face shape, camera pose, albedo map, and SH lighting coefficients given a face image.

For our light encoding \mathbf{l} , we directly use the SH coefficients from DECA, consisting of 9 coefficients for each channel of the RGB. DECA’s 3D face shape is parameterized based on FLAME model [36] as blendshapes with three linear bases for identity shape, pose, and expression. Their respective coefficients are denoted by β, θ, ψ . Our face shape encoding \mathbf{s} is the combined $(\beta, \theta, \psi) \in \mathbb{R}^{|\beta|+|\theta|+|\psi|}$. DECA assumes orthographic projection and models the camera pose with isotropic scaling and 2D translation. We combine the scaling and translation parameters into $\mathbf{cam} \in \mathbb{R}^{1+2}$. Note that we do not use the predicted albedo map, as its estimation by DECA can be unreliable and was found empirically unnecessary.

Identity encoding (ξ). To help preserve the input’s identity, we use ArcFace [10], a pretrained face recognition model based on ResNet [23]. This model has been shown to produce discriminative and identity-preserving feature embeddings.

Cast shadow encoding (c). This scalar describes the intensity of visible cast shadows, typically caused by a dominant point or directional light source, such as the sun.

We trained a model to estimate c from a face image ourselves and fixed this pretrained estimator. To do this, we manually labeled around 1,000 face images with binary flags indicating whether cast shadows are visible. Following a technique proposed in DiffAE [56], we first use DiffAE’s pretrained encoder to map each face image to a semantically

meaningful latent code \mathbf{z} and train a logistic regression classifier on \mathbf{z} to predict the flag c is then computed as the logit value of the logistic regression. As shown in [56], this technique helps reduce the number of training examples required to achieve good accuracy, but we note that c can be estimated in other ways, such as with a CNN.

Background encoding (\mathbf{bg}). To help fix the background during relighting, we condition DDIM with an image of the input’s background detected by a face segmentation algorithm [97]. The ears, hair, and neck are excluded from the background and can still be relit by our algorithm (Figure 13).

D. DiFaReli: DDIM decoder & Modulator network

Our main network is a conditional DDIM that decodes our feature vector (with modified lighting information) to a relit version of the input image. In practice, the feature vector is used to *condition* the DDIM that maps $\mathbf{x}_T \sim \mathcal{N}(\mathbf{0}, \mathbf{I})$ to the original input \mathbf{x}_0 during training or maps $\mathbf{x}_T = \text{DDIM}^{-1}(\mathbf{x}_0)$ from reversing the generative process to the relit output during relighting (Section III-G). This conditioning involves another network called *Modulator* network, which converts the light, shape, and camera encodings into spatial modulation weights for the DDIM decoder.

The architecture of the DDIM decoder is based on Dhariwal et al. [12], which is a modified UNet built from a stack of residual blocks interleaved with self-attention layers (full details in Appendix III).

E. DiFaReli: Conditioning DDIM decoder

Conditioning a diffusion model on a condition vector can be done in various ways, such as through adaptive group normalization [93], [56], [12] or attention-based mechanisms [49], [64], among others. In our problem, the lighting information is encoded explicitly as SH coefficients and their interaction with 3D shape, specifically the surface normals, can be precisely modeled with the SH lighting equation. Our idea is to ease the modeling of the known interaction by rendering a shading reference of the target relit face. The primary goal of this reference is to convey the information about the target lighting and shading in a spatially-aligned manner, not the geometry or the exact shading intensities. The following sections detail this “spatial” conditioning technique as well as a standard non-spatial conditioning technique used for other encodings.

Spatial conditioning. This technique is used for the light, shape, camera and background encodings ($\mathbf{l}, \mathbf{s}, \mathbf{cam}, \mathbf{bg}$). Given the face shape \mathbf{s} , we first convert it to a triangle mesh using the three linear bases of FLAME model [36] and remove the ears, eyeballs, neck, and scalp from the mesh to retain only the face region (See Figure 2). We remove those parts because they are often inaccurate and hard to estimate correctly (e.g., occluded ears behind hair). We assume a constant gray albedo (0.7, 0.7, 0.7) and render this mesh in the camera pose described by \mathbf{cam} with surface colors computed with \mathbf{l} using the standard SH lighting equation. The details are in Appendix IV, and we discuss this albedo choice and the inherent albedo-light ambiguity in Section VI.

Then, this shading reference R , which shows a shaded face in the shape and pose of the input person under the target lighting, is concatenated with the background image \mathbf{bg} and fed to the Modulator network. Let us denote the output of each residual block i in the Modulator network by $\mathbf{m}_i \in \mathbb{R}^{H_i \times W_i \times D_i}$, and the output of the corresponding residual block in the identical DDIM’s first half by $\mathbf{o}_i \in \mathbb{R}^{H_i \times W_i \times D_i}$. In the DDIM, we take each residual block’s output \mathbf{o}_i and replace it with \mathbf{o}'_i , which will be used as input to the subsequent layer in the network:

$$\mathbf{o}'_i = \mathbf{o}_i \odot \tanh(\mathbf{m}_i), \quad (2)$$

where \odot is the element-wise multiplication. This conditioning technique allows the shaded image R and the background to retain their spatial structure and facilitate local conditioning of the generation as they are spatially aligned with the input (e.g., their facial parts and background are in the same positions).

Non-spatial conditioning. This technique is used for $(\mathbf{s}, \mathbf{cam}, \boldsymbol{\xi}, c)$. The direct use of \mathbf{s}, \mathbf{cam} again in this technique is empirically found to be helpful, in addition to their indirect use through the shading reference. We use a similar conditioning technique as used in [12], [56] based on adaptive group normalization (AdaGN) [93] for these encodings and also for the time embedding in the standard diffusion model training $\gamma(t)$, where γ is a sinusoidal encoding function [12]. Given an input feature map $\mathbf{h}_j \in \mathbb{R}^{H_j \times W_j \times D_j}$, we compute

$$\text{AdaGN}_j(\mathbf{h}_j, \mathbf{s}, \mathbf{cam}, \boldsymbol{\xi}, c, t) = \mathbf{k}_j(\mathbf{t}_j^s \text{GN}(\mathbf{h}_j) + \mathbf{t}_j^b), \quad (3)$$

where $\mathbf{k}_j = \text{MLP}_j^3(\text{Concat}(\mathbf{s}, \mathbf{cam}, \boldsymbol{\xi}, c)) \in \mathbb{R}^{D_j}$ is the output of a 3-layer MLP with the SiLU activation [14], and $(\mathbf{t}_j^s, \mathbf{t}_j^b) \in \mathbb{R}^{2 \times D_j} = \text{MLP}_j^1(\gamma(t))$ is the output from a single-layer MLP also with the SiLU activation. GN is the standard group normalization. We apply our AdaGN in place of all the AdaGNs in the original architecture of [12], which occur throughout the UNet (Details in Appendix III).

F. DiFaReli: Training

We jointly train the DDIM decoder, parameterized as a noise prediction network ϵ_θ , and the Modulator network $M_\phi(\mathbf{l}, \mathbf{s}, \mathbf{cam}, \mathbf{bg})$ using standard diffusion training [25], [78], [56]. Here we consider the MLPs in Figure 2 as part of the DDIM. We adopt the simplified, re-weighted version of the variational lower bound with ϵ parameterization:

$$L_{\text{simple}} = \mathbb{E}_{t, \mathbf{x}_0, \epsilon} \|\epsilon_\theta(\mathbf{x}_t, t, M_\phi, \mathbf{s}, \mathbf{cam}, \boldsymbol{\xi}, c) - \epsilon\|_2^2, \quad (4)$$

where ϵ_θ is trained to predict the added noise $\epsilon \sim \mathcal{N}(\mathbf{0}, \mathbf{I})$ in $\mathbf{x}_t = \sqrt{\alpha_t} \mathbf{x}_0 + \sqrt{1 - \alpha_t} \epsilon$, given a training image \mathbf{x}_0 . We define α_t as $\prod_{s=1}^t (1 - \beta_s)$, where β_t is the noise level at timestep t in the Gaussian diffusion process $q(\mathbf{x}_t | \mathbf{x}_{t-1}) = \mathcal{N}(\sqrt{1 - \beta_t} \mathbf{x}_{t-1}, \beta_t \mathbf{I})$. We use a linear noise schedule and a total step $T = 1000$. Note that we do not reverse $\mathbf{x}_T = \text{DDIM}^{-1}(\mathbf{x}_0)$ during training.

G. DiFaReli: Relighting

To relight an input image, we first encode the input image into our feature vector \mathbf{f} (Equation 1), then reverse the deter-

ministic generative process of our DDIM conditioned on \mathbf{f} , starting from the input image \mathbf{x}_0 to $\mathbf{x}_{T=1000}$.

$$\mathbf{x}_{t+1} = \sqrt{\alpha_{t+1}} \mathbf{g}_\theta(\mathbf{x}_t, t, \mathbf{f}) + \sqrt{1 - \alpha_{t+1}} \epsilon_\theta(\mathbf{x}_t, t, \mathbf{f}), \quad (5)$$

where \mathbf{g}_θ represents the predicted \mathbf{x}_0 , which is reparameterized from ϵ_θ and is computed by:

$$\mathbf{g}_\theta(\mathbf{x}_t, t, \mathbf{f}) = \frac{1}{\sqrt{\alpha_t}} (\mathbf{x}_t - \sqrt{1 - \alpha_t} \epsilon_\theta(\mathbf{x}_t, t, \mathbf{f})). \quad (6)$$

After obtaining \mathbf{x}_T , we modify the SH light encoding \mathbf{l} and the cast shadow flag c to the target \mathbf{l}' and c' , which can be set manually or inferred from a reference lighting image using DECA and our cast shadow estimator. Then, we decode the modified $\mathbf{f}' = (\mathbf{l}', \mathbf{s}, \mathbf{cam}, \boldsymbol{\xi}, c', \mathbf{bg})$ using the reverse of Equation 5, starting from \mathbf{x}_T to produce the final output.

The reverse process to obtain \mathbf{x}_T is key to reproducing high-frequency details from the input image. As demonstrated in DiffAE [56], DDIM will encode any information not captured in the conditioning feature vector \mathbf{f} in the noise map \mathbf{x}_T . This information includes high-frequency details, such as the hair pattern or skin texture.

Improved DDIM sampling with mean-matching. We observe that when the input image contains a background with extreme intensities (e.g., too dark or too bright), DDIM can produce results with a slight change in the overall brightness. We alleviate this issue by computing the mean pixel difference between each \mathbf{x}_t during DDIM’s generative reversal ($\mathbf{x}_0 \rightarrow \mathbf{x}_T$) and \mathbf{x}_t from self-decoding of the reversed noise \mathbf{x}_T . This sequence of mean differences is then applied to the decoding for relighting (Appendix II).

IV. DiFaReli++: SINGLE-SHOT FACE RELIGHTING WITH CONSISTENT CAST SHADOWS

We present three improvements to DiFaReli [54]: 1) the generation of consistent cast shadows under dynamic lighting, 2) extension of relighting to non-facial parts (e.g., clothes, earrings, hats), and 3) single-shot face relighting.

A. Face relighting with consistent cast shadows.

To enable relighting with consistent cast shadows, we build on the idea of DiFaReli, which achieves relighting by conditioning a DDIM with lighting information. Here, the idea is to extend the lighting condition to include more comprehensive shadow information beyond the single scalar shadow flag used in DiFaReli (Section III-C). Specifically, we use a binary shadow map to specify the face areas under cast shadows. Once the network learns to utilize this shadow conditioning, the relit output will feature realistic cast shadows that align with the provided shadow map under the target lighting.

The key challenges are how to estimate the shadow map of the input image for training and the target shadow map under the target lighting for inference. For this idea to work, the shadow maps used for training need to be highly accurate and spatially aligned with the input’s shadows; otherwise, the network will disregard them as noisy and unhelpful for the reconstruction training objective. This requirement precludes

the use of ray tracing, as employed in prior work [28], which relies on accurate geometry to estimate accurate shadow maps.

To estimate shadow maps, we instead propose leveraging DiFaReli to transform the input image into versions with stronger and reduced cast shadows, then identify cast shadow areas through pixel differences (Figure 3). However, this technique can only be used for training but not inference, as the two versions have incorrect *target* lighting shadows. Fortunately, we can leverage a ray-traced shadow map at test time and produce consistent and plausible outputs. We next explain the process in detail.

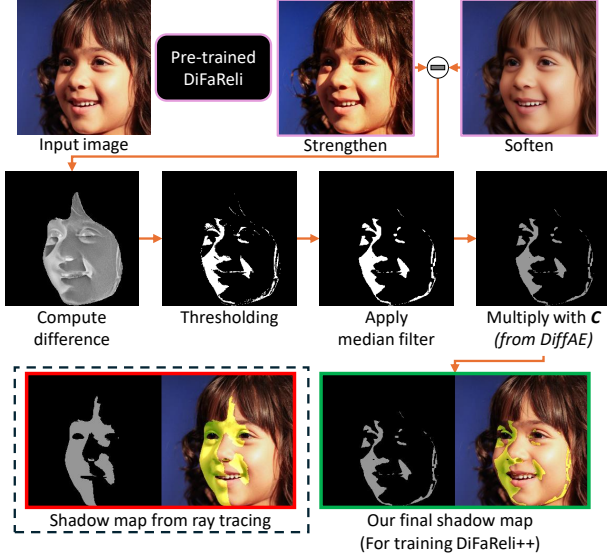


Fig. 3: **Computing the shadow map for training.** We used a pretrained DiFaReli model to relight an input image into two versions, one with stronger and one with reduced cast shadows, then identify shadow areas through pixel differences. Our process produces more accurate and spatially aligned shadow maps compared to ray-traced maps shown in red, which suffer from inaccurate lighting and geometry estimation.

1) *Computing a shadow map:* We use our pretrained DiFaReli model to relight an input image into two versions, one with stronger and one with reduced cast shadows, by setting the shadow value (c) to the maximum and minimum estimated shadow values across all training images. These values are estimated by DiffAE [56] on the FFHQ dataset as explained in Section III-C. We then compute the pixel difference between the two versions and apply thresholding to the difference map to create a binary mask, where 1 indicates cast shadow areas and 0 indicates non-shadow areas. By generating the two versions using consistent global maximum and minimum levels, we can determine a single threshold that works effectively across input images, despite variations in their original shadow intensities.

Next, we apply a median filter to remove small, isolated shadow regions from the thresholded shadow map. Finally, we multiply this map with a normalized shadow value (c) of the input image, resulting in a c -scaled shadow map that also encodes the shadow intensity.

2) *Training DiFaReli++ with cast shadows:* We concatenate the precomputed shadow map and the shading reference, feed them into the Modulator network, and follow DiFaReli’s training procedure.

3) *Inferencing DiFaReli++ with cast shadows:* Once our network learns to associate the estimated shadow map with the input image, we can guide it to generate new cast shadow effects using ray tracing. Specifically, we perform ray tracing on the estimated depth map from DECA, using the dominant light direction from SH, as described in [28]. We follow a similar relighting process to DiFaReli (see Section III-G), using the precomputed shadow map for inversion and the ray-traced shadow map for generation. Note that if we had used the ray-traced shadow map for inversion, this would result in over-brightening artifacts and the failure to remove certain shadowed areas (Figure 46 in the Appendix). This suggests that the network may misinterpret shadow areas in the input image, resulting in unintended brightening during relighting.

B. Relighting of non-facial parts.

Another goal is to expand the relightable area of DiFaReli beyond facial parts (e.g., face, neck, and hair) to other areas of the person, such as clothes, earrings, and hats, but not the rest of the background. In the original DiFaReli, these non-facial parts remain unchanged because the network is conditioned on the background encoding (bg), which contains their raw pixels. However, simply removing this condition can lead to structural changes in those parts, as shown in Figure 13, while still not allowing us to relight them.

To address this, we condition the network with a set of segmentation masks instead of the background encoding. This approach makes the conditioning less restrictive and still enables relighting while preserving the structure of each part. These masks are computed using Bisenet face parsing [97] and correspond to facial parts such as the eyes, nose, mouth, as well as non-facial parts such as the hair and neck, covering 14 distinct areas (Figure 47). Finally, we feed a concatenation of these masks, a shadow map, and a shading reference as input to the Modulator network (See Figure 4).

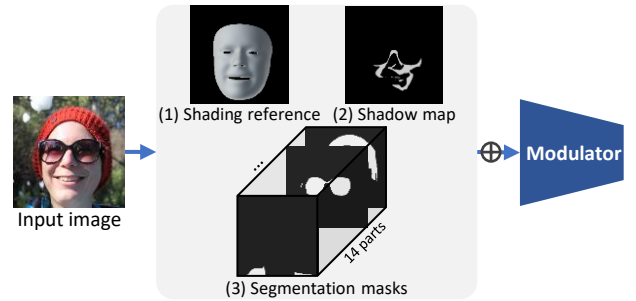


Fig. 4: **Modifications of the Modulator’s input in DiFaReli++.** The input is a concatenation of the shadow map, the shading reference, and segmentation masks (see all masks in Figure 47). This modification allows generation of consistent cast shadows and enables relighting of non-facial parts.

C. DiFaReli++_{ss}: Single-shot face relighting network

Currently, both DiFaReli [54] and DiFaReli++ with controllable cast shadows take approximately 3 minutes to relight a

single input image. To improve speed, the idea is to use our pretrained DiFaReli++ to generate synthetic relit pairs and use them to train a relighting network in a supervised manner. This network adopts the same architecture as DiFaReli++ and requires only a single network pass to relight an input image, given the required pre-processed data (e.g., DECA and shadow map), without relying on diffusion sampling or DDIM inversion. As in DiFaReli and DiFaReli++, this pre-processed data needs to be computed only once per input face image and can be reused for each relighting process. Surprisingly, the resulting single-shot network, referred to as DiFaReli++_{ss}, is not only three orders of magnitude faster but also achieves better scores across all metrics than DiFaReli++, which was used to generate the synthetic training data (Figure 12). We next describe the dataset generation and training process (see Figure 5 for an overview).

1) *Dataset generation*: The training set for DiFaReli++_{ss} was created by uniformly sampling pairs of face images from all 60,000 images of the FFHQ training set. In each pair, we use one face image as input and use the lighting condition from the other image as the target lighting. The lighting condition is estimated with DECA [16]. Then, we relight the input under the target lighting using DiFaReli++, resulting in 60,000 pairs of (input, relit input) along with their corresponding shading references and shadow maps.

2) *Training*: DiFaReli++_{ss} uses a similar architecture to DiFaReli, including the Modulator network, except that the Modulator takes two sets of inputs (8 channels in total), each comprising a shading reference (3 channels) and an estimated shadow map scaled by c (1 channel) of the input image. The first set uses the input’s own lighting condition, while the second set corresponds to the target lighting condition. We train the network using a simple L2 loss between the predicted image and the synthetic “ground-truth” image.

3) *Relighting*: We feed an input image and its encodings to the network along with the two sets of shading references and shadow maps for the Modulator, following the same input preprocessing as in training.

V. EXPERIMENTS

In this section, we present quantitative and qualitative results of our proposed method. We provide a comparison of our relighting performance with state-of-the-art methods on the Multi-PIE dataset (Section V-A), a runtime comparison (Section V-B), a user study on the FFHQ dataset (Section V-C), and ablation studies on the conditioning mechanisms (Section V-E). Implementation and dataset details are in Appendix II.

Evaluation metrics. We use DSSIM [48], LPIPS [101], and MSE. DSSIM measures structural dissimilarity, while LPIPS measures perceptual quality. All metrics are computed between each relit image and its ground-truth image only on the face region, following [28], [29] using the same face parsing algorithm [97].

A. Relighting performance

We evaluate our relighting performance on the Multi-PIE dataset [21] against recent state-of-the-art methods [29], [28],

[48], [51], [13], [100], [54], [22]. Note that several prior works [51], [100], [13], [61], [46], [22] tackle different problem setups: [13] requires a photo album of the same subject (≈ 20 images) to fine-tune a personalized model, which our setting lacks. [22] aims to animate and relight a single portrait image given target keypoints and lighting. Other methods [51], [46], [34] require an HDR environment map as input, which must first be estimated from a target image, while [100], [61] require a background image as input. These make comparisons with [51], [46], [13], [100], [61], [22] not entirely apples-to-apples.

In our experiments, we used the pretrained Stage 1 model from DiffusionRig [13] without any finetuning, as the fine-tuned model (Stage 2) requires a subject-specific photo collection, which was not available in our single-image setting. Additionally, the authors of [13] show that fine-tuning on a single image struggles to adapt to new lighting conditions (see Figure 7 in [13]). For the relightable keypoint-based portrait animation technique [22], we modified the input by using the keypoints of the input image as the target, which disables portrait animation and thus limits control to relighting only (see Figure 49 in the Appendix for the modified input).

We also provided each method with its required target lighting. Pandey et al. [51] used their own light estimator to generate a target HDR map from a target image. Zhang et al. [100] do not include a light estimator and instead require a target background. Thus, we provided a proxy background as the target lighting, created by unwrapping a rendered sphere under the target SH lighting. Examples of the proxy backgrounds are shown in Figure 48 (Appendix). All results for [51] were generated by the authors themselves, and the results for [100] were generated using their official code. Test sets and code of [46], [61], [34] were not released. Instead, we provide a qualitative comparison with [46], [34] using their input images, target lighting, and results cropped directly from their papers (see Section VI-A for details and results).

Our experiment has two setups for the target lighting:

i). From the same person. This setup uses the same test set as [29], which contains 862 testing samples from 329 subjects.

ii). From a different person. This setup contains 200 random triplets of input, target, and ground-truth images, where the target image is of a different person.

The results are shown in Table I and Figure 7. For both setups, our method achieves the best performance across all metrics with minimal artifacts and convincingly relights areas like the neck and ears or removes cast shadows, such as the shadow from the nose of the lady in Figure 7. We include a comparison with [72], [105], [81] in Appendix VI.

B. Runtime improvement

We compare our single-shot network against three training-free diffusion acceleration techniques: DPM-Solver [41], DPM-Solver++ [42], and UniPC [104], each offering a variable trade-off between sampling speed and quality. We apply these techniques to our pretrained DiFaReli++ model and report DSSIM, MSE, and LPIPS scores for various numbers of sampling steps in Figure 12. All solvers use a multistep schedule and their orders are set to 2.

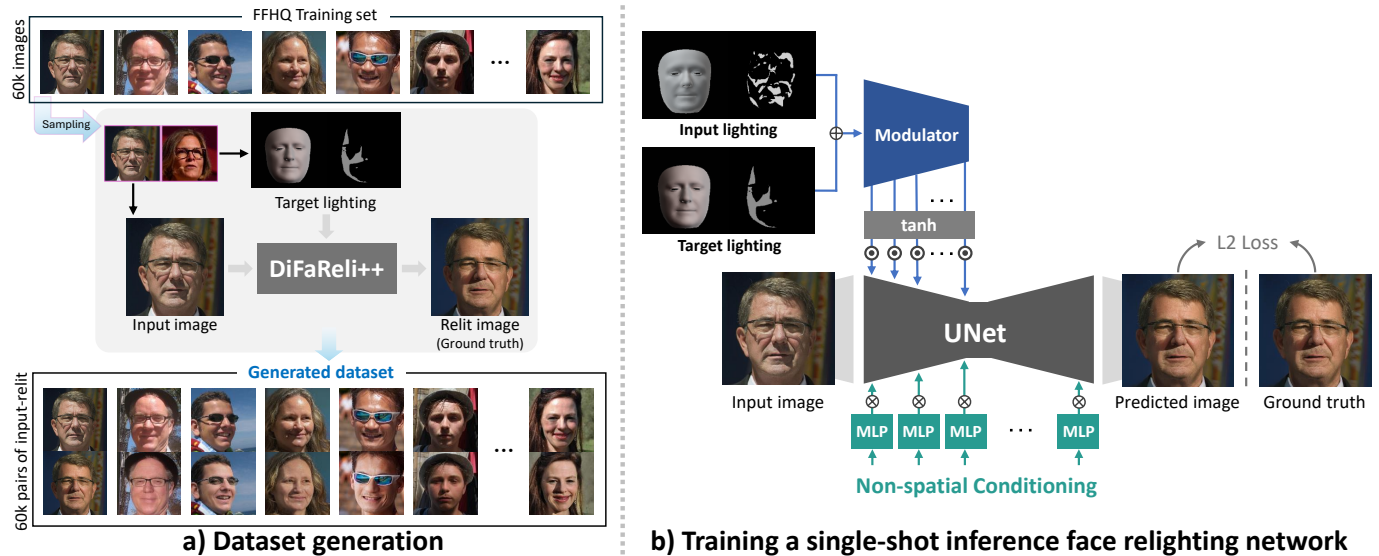


Fig. 5: **Single-shot face relighting framework** involves a) using DiFaReli++ to generate supervised relit pairs and b) training a single-shot relighting network with the same architecture as DiFaReli++ using the training pairs with a simple L2 loss.



Fig. 6: **Relit results on FFHQ [32]**, a dataset of diverse face images captured in real-world conditions. Our method produces more realistic shading and controllable cast shadows (via the shadow map in the rightmost column), effectively removing existing shadows and adding new ones. It also relights non-facial parts (e.g., hats, hoodies, or shirts) to match the target lighting, enhancing overall realism. Unlike DiFaReli++, DiffusionRig[13] fails to preserve identity, as it relies on subject-specific fine-tuning on a personal photo collection, making it unsuitable for single-image relighting. For [22], [13], we also performed a grid search over their relighting hyperparameters to verify that the oversaturation artifacts were not caused by suboptimal tuning (see Figures 40-43). Additional results are in Appendix (Figures 30, 31, 32, and 33).

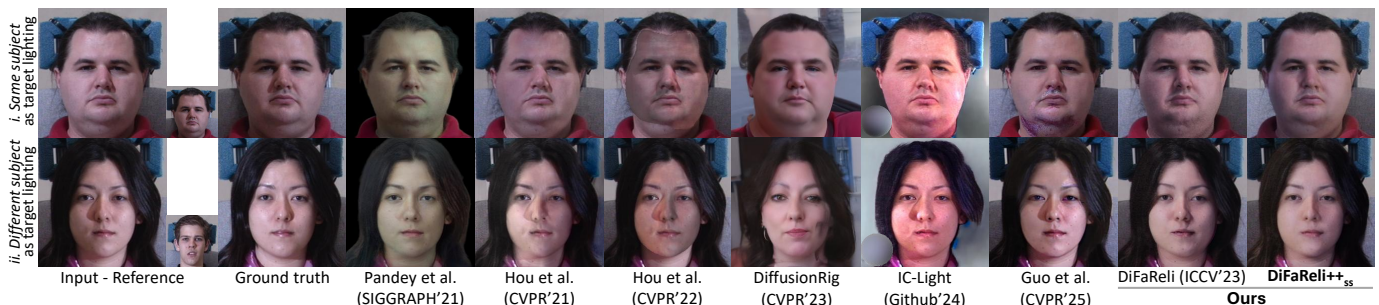


Fig. 7: **Relighting results on Multi-PIE [21]** when the target lighting is taken from the same person (first row) and from a different person (second row).

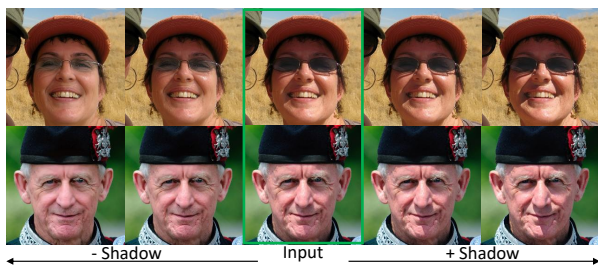


Fig. 8: **Varying intensities of cast shadows.** DiFaReli’s ability to change the intensity of cast shadows by adjusting the scalar c and decode the modified feature vector (more in Figure 45).

TABLE I: State-of-the-art comparison on Multi-PIE.

Method	DDSIM↓	MSE↓	LPIPS↓
i). Same subject as target lighting			
Nestmayer et al. [48]	0.2226	0.0588	0.3795
Pandey et al. (Total Relighting) [51]	0.0875	0.0165	0.2010
Hou et al. [29]	0.1186	0.0303	0.2013
Hou et al. [28]	0.0990	0.0150	0.1622
Ding et al. (DiffusionRig) [13]	0.0870	0.0098	0.2098
Zhang et al. (IC-Light) [100]	0.1978	0.0499	0.1887
Guo et al. [22]	0.1088	0.0234	0.1733
Ours (DiFaReli)	0.0711	0.0122	0.1370
Ours (DiFaReli++)	0.0604	0.0090	0.1043
Ours (DiFaReli++_{ss})	0.0590	0.0075	0.1023
ii). Different subject as target lighting			
Pandey et al. (Total Relighting) [51]	0.1000	0.0252	0.2053
Hou et al. [29]	0.1056	0.0247	0.1989
Hou et al. [28]	0.1150	0.0238	0.2215
Ding et al. (DiffusionRig) [13]	0.1130	0.0180	0.2292
Zhang et al. (IC-Light) [100]	0.2239	0.0654	0.2102
Guo et al. [22]	0.1230	0.0255	0.1869
Ours (DiFaReli)	0.0969	0.0215	0.1669
Ours (DiFaReli++)	0.0824	0.0169	0.1223
Ours (DiFaReli++_{ss})	0.0801	0.0148	0.1123

We measured the time required for network inference alone, assuming all one-time pre-processed data (e.g., DECA, shadow difference map) is provided. Our method runs in 0.07 seconds and outperforms three acceleration techniques at 10 sampling steps across all metrics, while those techniques already take over one second to run. Increasing the sampling steps further (e.g., to 100) for those techniques can improve their quality but slows down runtime by two orders of magnitude (13.56s). Conversely, reducing the steps below 10 can speed up these techniques but the quality would become extremely poor. Surprisingly, the single-shot DiFaReli++_{ss} also outperforms the original DiFaReli++ across all metrics, even though it was trained on synthetic data generated by DiFaReli++. The improvement may result from the single-shot model directly learning image relighting, whereas the original model must disentangle light information and perform DDIM inversion for relighting, which are more complex and prone to errors.

C. User study

In addition to the quantitative evaluation, we conducted three user studies to assess relighting quality, as follows:

1) *Relighting quality on facial and non-facial parts:* This study comprises 100 input images, another 100 images serving as target lighting, and 100 relit results from each method. The input and target lighting images are randomly selected from the FFHQ test set. For each input image, we generated

relit results using six recent state-of-the-art baselines [100], [29], [28], [13], [51], [22] and our method. We then asked 30 participants to choose the result that most convincingly relights the input image to match the target lighting, considering: (1) only the face, and (2) the entire person, including both facial and non-facial parts but excluding the background. In total, we received 600 responses (100 inputs, 2 questions per input, 3 participants per question).

2) *Relighting quality under moving lights:* This study examines relighting quality under dynamic lighting conditions, enabling users to assess the temporal consistency of cast shadows. We compare our method against five recent state-of-the-art baselines [100], [29], [28], [13], [22] using 20 randomly selected input images from the FFHQ test set. For each input, we generate two 60-frame videos for each method by rotating the input’s SH lighting 360 degrees, one around the up axis (yaw) and the other around the forward axis (roll). We then asked 30 participants to choose the video that most convincingly relights the input image with realistic cast shadow effects and consistent shadow movement. We received 600 responses (20 inputs, 2 questions per input, 15 participants per question).

3) *Relighting quality under rotating HDR environment maps:* To compare with [31], we randomly selected three HDR maps from its official repository and rotated them around the yaw and roll axes (similar to Section V-C2). We evaluated on 20 randomly selected FFHQ test inputs, collecting a total of 1,800 responses (3 HDR maps, 20 inputs, 2 questions, 15 participants).

In all studies, we compared each method in a 1-vs-1 manner. All images and videos are in 256x256 resolution. The interfaces used on Amazon Turk are shown in Figures 50, 51, and 52 (Appendix). The study results are reported in Table II, with qualitative examples provided in Figures 6, 9, and 10. Our method was the most preferred across all scenarios in all studies, with average preference rates of 0.70 vs. 0.30 for relighting quality on facial and non-facial parts, 0.72 vs. 0.28 under moving lights, and 0.65 vs. 0.35 under rotating HDR environment maps.

TABLE II: **User study results.** Percentage of times other methods were preferred over ours in 1-vs-1 comparisons (details are provided in Sections V-C1–V-C3).

Method	Relit area (V-C1)			Light rotation (V-C2)		
	Face	Non-face	Avg.	Yaw	Roll	Avg.
Pandey et al. [51]	29%	22%	26%	-	-	-
Hou et al. [29]	38%	40%	39%	27%	32%	29%
Hou et al. [28]	25%	22%	24%	31%	32%	32%
Ding et al. [13]	36%	34%	35%	27%	28%	28%
Zhang et al. [100]	29%	26%	28%	34%	28%	31%
Guo et al. [22]	34%	31%	32%	24%	21%	22%

Method	HDR rotation (V-C3)		
	Yaw	Roll	Avg.
Jin et al. [31]	37%	33%	35%

D. Qualitative evaluations

Relighting on FFHQ dataset. In Figure 6, we present a qualitative comparison with seven recent state-of-the-art meth-

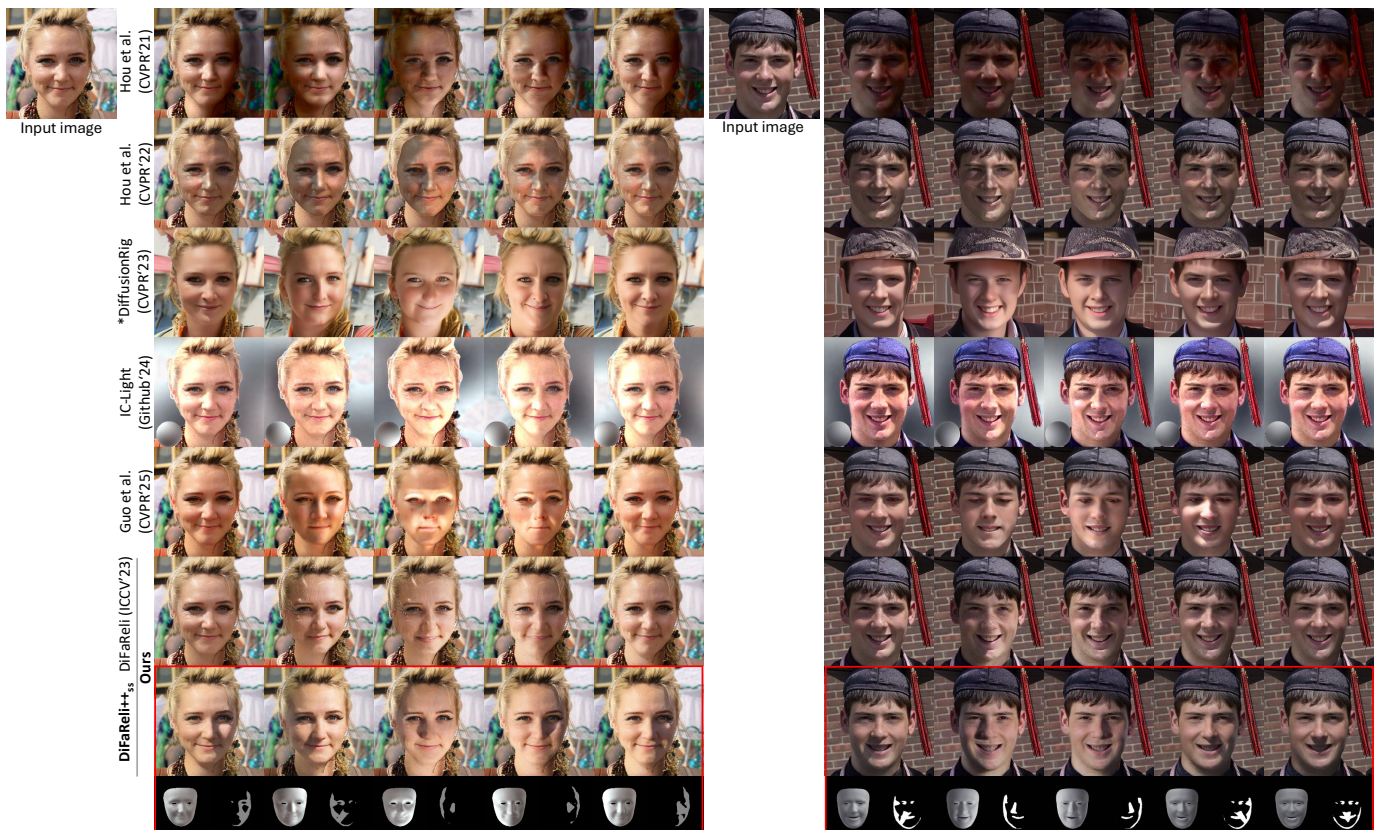


Fig. 9: **Relighting with consistent cast shadows under moving lights.** Compared to six recent state-of-the-art methods [100], [29], [28], [13], [54], [22], DiFaReli++ effectively removes input cast shadows and synthesizes new ones in a realistic and consistent manner. *DiffusionRig [13] was designed for fine-tuning on a personal photo collection, but since our single-image relighting setup lacks such data, its results are generated without fine-tuning, leading to identity shift issues. We observed oversaturation in [22], [13], and performed a hyperparameter grid search to ensure it was not due to suboptimal tuning (see Figures 36-39). The bottom row shows our shading references and shadow maps. Additional results are provided in the Appendix (Figures 25, 26, 27, 28, and 29).

ods [51], [29], [28], [13], [100], [22], [54] on subjects with different genders, races, accessories, and clothing. Our approach produces highly realistic results by effectively handling facial highlights, removing hard shadows and those cast by external objects (Figure 14) while simultaneously synthesizing new cast shadows guided by the provided shadow map. In contrast, competing methods often leave behind shadow or shading residuals due to inaccurate albedo predictions for these in-the-wild images. Furthermore, unlike [54], which focuses primarily on the face, our method can realistically relight both the face and clothing to match the target lighting, further enhancing the realism.

Relighting with consistent cast shadows. In Figure 9 and Figures 25-29, we present a qualitative comparison assessing the consistency of cast shadows under moving light conditions on the FFHQ dataset [32] against six recent competing techniques [29], [28], [13], [100], [22], [54]. The input images for this comparison contain varying cast shadows, ranging from hard shadows caused by direct sunlight or a point light source to softer shadows produced under overcast conditions.

Moreover, we compared our method against the recent object-relighting technique, Neural Gaffer [31], as shown in Figure 10 and Figures 34 and 35 of the Appendix. Since this

method takes an HDR environment map as input, we rotated the map and rendered the corresponding shading reference for our method. While Neural Gaffer can relight facial images using an environment map, it is unable to remove existing cast shadows. In contrast, our approach removes such shadows more effectively and produces consistent cast shadow effects.

By leveraging a shadow map, DiFaReli++ can generate realistic and consistent cast shadows that align with a guided shadow map, extending the original DiFaReli’s capabilities (best observed in our supplementary videos).

Shadow flag condition. We show DiFaReli’s novel ability to adjust the strength of cast shadows on FFHQ [32] in Figure 8 by varying the cast shadow’s value (c). Our method can realistically remove or intensify shadows (e.g., those cast by eyeglasses or face geometry). DiFaReli++ offers similar control by scaling the shadow value used to scale the shadow map (Section IV-A1), as shown in our supplementary video.

E. Ablation studies

1) *Light conditioning:* We compare our full pipeline with two alternatives for conditioning the DDIM: a) Removing our Modulator network and directly feeding the reference shading to the DDIM by concatenating it with each x_t at every



Fig. 10: **Relighting comparison with a state-of-the-art object-relighting method, Neural Gaffer [31].** The top row shows input HDR maps, and below the results are our shading references and shadow maps. Following Neural Gaffer, the background is composited only for visualization. Neural Gaffer can brighten some regions but often fails to remove cast shadows, while DiFaReli++ effectively eliminates them and synthesizes consistent new ones. Fine-tuning Neural Gaffer for faces requires multi-view light stage data, which is hard to obtain and scale. More results are in Figures 34 and 35 in the Appendix.



Fig. 11: **Results using various acceleration techniques.** with different sampling steps on an input image from FFHQ. While these techniques can reduce the sampling steps, they introduce artifacts and blurriness. In contrast, our distilled version of DiFaReli++ (DiFaReli++_{ss}) delivers the highest quality, the least noisy output, and runs in just 0.07 seconds.

timestep; and b) Omitting the shading reference entirely and instead concatenating the light encoding \mathbf{l} with (s, cam, ξ, c) using the non-spatial conditioning technique.

We report the results in Table III and show a qualitative comparison in Appendix VI. Using the light encoding as part of a non-spatial vector (b) performs the worst among all three methods, while feeding the shading reference directly to the DDIM without our Modulator (a) shows improvement but still lags behind our proposed pipeline.

2) *Non-spatial conditioning*: In this section, we study the benefits of non-spatial, face-related conditions extracted from ArcFace (ξ) and DECA (s, cam) by evaluating the relight performance on: c) Our method with no s, cam, ξ . d) Our method with no s, cam . e) Our method with no ξ .

We report the results in Table III and a qualitative comparison in Appendix VI. Removing all of s, cam, ξ performs the worst, while removing s, cam but retaining ξ obtains a better MSE score. In contrast, our full pipeline outperforms these alternatives on both DDSIM and LPIPS metrics, aligning with

human perception.

TABLE III: Ablation study on conditioning inputs.

Method	DDSIM↓	MSE↓	LPIPS↓
Light conditioning			
a) No <i>Modulator</i>	0.0749	0.0081	0.0868
b) Used as non-spatial	0.0885	0.0098	0.0947
Ours (DiFaReli)	0.0670	0.0077	0.0789
Non-spatial condition vector			
c) No s, cam, ξ	0.0713	0.0082	0.0909
d) No s, cam	0.0674	0.0063	0.0846
e) No ξ	0.0686	0.0074	0.0847
Ours (DiFaReli)	0.0670	0.0077	0.0789

3) *Conditioning mechanism alternatives*: We compare our conditioning techniques with ControlNet [99], published concurrently with our conference version [54]. Unlike our modulator, which injects spatial conditioning directly into the UNet encoder, ControlNet injects it into the UNet *decoder*,

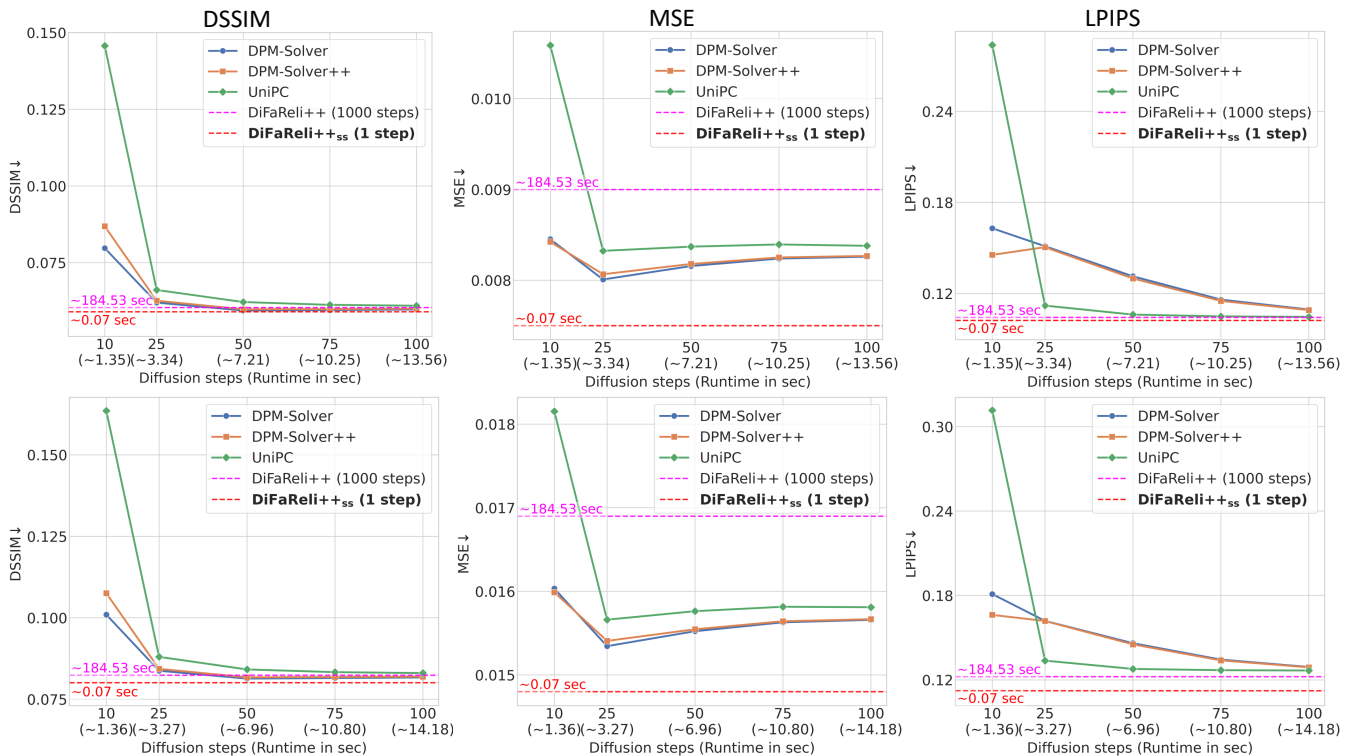


Fig. 12: **Trade-off between runtime and relighting performance of different acceleration techniques** measured on three metrics: DSSIM, MSE, and LPIPS. The **first row** shows results on the test set where the target lighting is taken from the same subject, while the **second row** uses target lighting from a different subject. The red dashed line represents our single-shot face relighting score (DiFaReli++_{ss}), and the magenta dashed line represents our original DiFaReli++ score.



Fig. 13: **Background conditioning ablation.** Without background conditioning, non-facial regions like hats may disappear. Conditioning on raw pixels in DiFaReli preserves the hat, while conditioning on segmentation masks in DiFaReli++_{ss} not only preserves it but also enables its relighting.

preceded by a zero-conv layer. For comparison, we replace our spatial conditioning (Modulator) with ControlNet and/or our non-spatial conditioning with a cross-attention layer, as used in Stable Diffusion (SD) [64] with ControlNet (see details in Section III-C). Unlike the original SD+ControlNet setup, where the pretrained SD model is frozen while ControlNet is being trained, we train both ControlNet and our diffusion model jointly from scratch to match our training objective. We evaluate on 100 randomly selected, disjoint self-target lighting pairs from Multi-PIE [21].

We report results in Table IV and show qualitative examples in Figures 21 and 22 (Appendix). Quantitatively, we found that the performance is broadly comparable, with our architecture performing slightly better. Using ControlNet for spatial conditioning (Rows a and b) often fails to change the skin tone to match the target lighting. However, we

TABLE IV: **Comparison on conditioning mechanism alternatives.** We replace DiFaReli++’s spatial and non-spatial components with ControlNet (CN) or Cross-attention (CA). (CN-mod) is ControlNet without its first convolutional block.

Conditioning Type		DDSIM↓	MSE↓	LPIPS↓
Spatial	Non-Spatial			
a) CN	CA	0.0983	0.0129	0.0868
b) CN	DiFaReli++	0.1014	0.0157	0.0840
c) CN-mod	CA	0.0697	0.0076	0.0751
d) DiFaReli++	CA	0.0694	0.0070	0.0695
e) DiFaReli++	DiFaReli++	0.0664	0.0044	0.0689

found that a simple modification that removes the initial zero convolutional block in ControlNet’s original design, denoted by CN-mod in Table IV, addresses the skin-tone matching problem (Figures 21) and further improves quantitative scores.

Regardless of these variations, our proposed shadow map conditioning is architecture-agnostic, enabling all combinations to generate cast shadows (Figure 22), suggesting adaptability to emerging backbones (e.g., DiTs [39], [103]).

VI. LIMITATIONS AND DISCUSSION

While our method produces photorealistic, plausible relit results with consistent cast shadows, the generated cast shadows may not always be physically accurate. Additionally, relighting to match a reference lighting image can be inaccurate as we rely on a light estimator to determine the target lighting. This



Fig. 14: **Improvements over DiFaReli’s failure cases.** DiFaReli++_{ss} better remove shadows cast by external objects (top) and better preserves sunglasses (bottom).

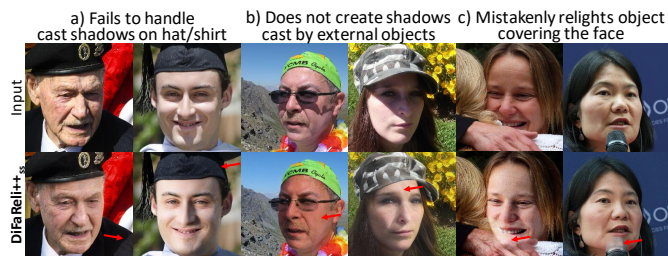


Fig. 15: **Failure cases.** Our method a) may fail to add or remove cast shadows on non-facial parts (e.g., hats, clothing), b) may not produce shadows cast by external objects, or c) may mistakenly relight objects occluding the face (e.g., hands), leading to unrealistic relighting in some cases.

process is susceptible to ambiguity where it is unclear whether a dark appearance is due to the skin tone or dim lighting. Other limitations (Figure 15) include mistakenly relit objects overlapping the face. Shadows cast by external objects (e.g., hats, glasses) are not generated, as our current shadow map is specific to the face area. While our method can relight non-facial areas by adjusting their shading, it often fails to synthesize or remove cast shadows from them.

Although our method, including the single-shot model, requires multiple conditionings (e.g., DECA, shadow map) to be pre-processed before relighting, this preprocessing is required only once per input image and can be reused indefinitely. Since our method does not rely on precise intrinsic decomposition, it opens up the possibility of extending relighting to full human bodies, objects, or scenes, where such decomposition is more challenging and prone to errors. Additionally, exploring alternative lighting models, such as HDRI, could also further enhance the framework’s capabilities.

VII. CONCLUSION

We present a diffusion-based face relighting method that eliminates the need for accurate intrinsic decomposition and can be trained on 2D images without requiring multiview images, relit pairs, light stage data, or 3D ground truth. Our key component is a conditional diffusion implicit model and a novel conditioning technique that maps a disentangled light representation to a relit image. This extended paper enhances the realism and consistency of cast shadows while expanding relightable regions to non-facial areas using segmentation masks and a shadow map estimated by our novel method.

Moreover, we distill our method into a single-shot relighting network that runs in a single network pass and even surpasses the teacher model. Our method achieves state-of-the-art results and produces highly photorealistic outputs with temporally consistent cast shadows in real-world scenarios.

REFERENCES

- [1] Tomer Amit, Eliya Nachmani, Tal Shaharbany, and Lior Wolf. Segdiff: Image segmentation with diffusion probabilistic models. *arXiv:2112.00390*, 2021. 19
- [2] Yogesh Balaji, Seungjun Nah, Xun Huang, Arash Vahdat, Jiaming Song, Karsten Kreis, Miika Aittala, Timo Aila, Samuli Laine, Bryan Catanzaro, et al. ediffi: Text-to-image diffusion models with an ensemble of expert denoisers. *arXiv:2211.01324*, 2022. 19
- [3] Fan Bao, Chongxuan Li, Jun Zhu, and Bo Zhang. Analytic-dpm: an analytic estimate of the optimal reverse variance in diffusion probabilistic models. *arXiv:2201.06503*, 2022. 4
- [4] Dmitry Baranchuk, Ivan Rubachev, Andrey Voynov, Valentin Khruikov, and Artem Babenko. Label-efficient semantic segmentation with diffusion models. *arXiv:2112.03126*, 2021. 19
- [5] Jonathan T Barron and Jitendra Malik. Shape, illumination, and reflectance from shading. *IEEE transactions on pattern analysis and machine intelligence*, 37(8):1670–1687, 2014. 1, 3
- [6] Volker Blanz and Thomas Vetter. A morphable model for the synthesis of 3d faces. In *Proceedings of the 26th annual conference on Computer graphics and interactive techniques*, pages 187–194, 1999. 3, 19
- [7] Eric R. Chan, Connor Z. Lin, Matthew A. Chan, Koki Nagano, Boxiao Pan, Shalini De Mello, Orazio Gallo, Leonidas Guibas, Jonathan Tremblay, Sameh Khamis, Tero Karras, and Gordon Wetzstein. Efficient geometry-aware 3d generative adversarial networks, 2022. 4
- [8] Chen-Hao Chao, Wei-Fang Sun, Bo-Wun Cheng, Yi-Chen Lo, Chia-Che Chang, Yu-Lun Liu, Yu-Lin Chang, Chia-Ping Chen, and Chun-Yi Lee. Denoising likelihood score matching for conditional score-based data generation. *arXiv:2203.14206*, 2022. 19
- [9] Florinel-Alin Croitoru, Vlad Hondru, Radu Tudor Ionescu, and Mubarak Shah. Diffusion models in vision: A survey. *arXiv:2209.04747*, 2022. 19
- [10] Jiankang Deng, Jia Guo, Niannan Xue, and Stefanos Zafeiriou. Arcface: Additive angular margin loss for deep face recognition. In *Proceedings of the IEEE/CVF conference on computer vision and pattern recognition*, pages 4690–4699, 2019. 2, 5, 19
- [11] Yu Deng, Jiaolong Yang, Sicheng Xu, Dong Chen, Yunde Jia, and Xin Tong. Accurate 3d face reconstruction with weakly-supervised learning: From single image to image set. In *Proceedings of the IEEE/CVF Conference on Computer Vision and Pattern Recognition Workshops*, pages 0–0, 2019. 19
- [12] Prafulla Dhariwal and Alexander Nichol. Diffusion models beat gans on image synthesis. *Advances in Neural Information Processing Systems*, 34:8780–8794, 2021. 5, 6, 18, 19, 21
- [13] Zheng Ding, Cecilia Zhang, Zhihao Xia, Lars Jebe, Zhuowen Tu, and Xiuming Zhang. Diffusionrig: Learning personalized priors for facial appearance editing. In *Proceedings of the IEEE/CVF Conference on Computer Vision and Pattern Recognition*, 2023. 3, 8, 9, 10, 11, 20, 39, 40, 42
- [14] Stefan Elfving, Eiji Uchibe, and Kenji Doya. Sigmoid-weighted linear units for neural network function approximation in reinforcement learning. *Neural Networks*, 107:3–11, 2018. 6
- [15] Qianli Feng, Viraj Shah, Raghudeep Gadde, Pietro Perona, and Aleix Martinez. Near perfect gan inversion. *arXiv:2202.11833*, 2022. 4
- [16] Yao Feng, Haiwen Feng, Michael J. Black, and Timo Bolkart. Learning an animatable detailed 3D face model from in-the-wild images. volume 40, 2021. 2, 4, 5, 8, 21, 22
- [17] Yao Feng, Haiwen Feng, Michael J Black, and Timo Bolkart. Learning an animatable detailed 3d face model from in-the-wild images. *ACM Transactions on Graphics (ToG)*, 40(4):1–13, 2021. 19
- [18] David Futschik, Kelvin Ritland, James Vecore, Sean Fanello, Sergio Orts-Escobedo, Brian Curless, Daniel Sýkora, and Rohit Pandey. Controllable light diffusion for portraits, 2023. 3
- [19] Kyle Genova, Forrester Cole, Aaron Maschinot, Aaron Sarna, Daniel Vlasic, and William T Freeman. Unsupervised training for 3d morphable model regression. In *Proceedings of the IEEE Conference on Computer Vision and Pattern Recognition*, pages 8377–8386, 2018. 19
- [20] Ian Goodfellow, Jean Pouget-Abadie, Mehdi Mirza, Bing Xu, David Warde-Farley, Sherjil Ozair, Aaron Courville, and Yoshua Bengio. Generative adversarial networks. *Communications of the ACM*, 63(11):139–144, 2020. 4

- [21] Ralph Gross, Iain Matthews, Jeffrey Cohn, Takeo Kanade, and Simon Baker. Multi-pie. *Image and vision computing*, 2010. **3, 8, 9, 13, 18, 24**
- [22] Mingtao Guo, Guanyu Xing, and Yanli Liu. High-fidelity relightable monocular portrait animation with lighting-controllable video diffusion model. In *Proceedings of the Computer Vision and Pattern Recognition Conference (CVPR)*, pages 228–238, June 2025. **3, 8, 9, 10, 11, 20, 37, 38, 40, 41, 45**
- [23] Kaiming He, Xiangyu Zhang, Shaoqing Ren, and Jian Sun. Deep residual learning for image recognition. In *2016 IEEE Conference on Computer Vision and Pattern Recognition (CVPR)*, 2016. **5**
- [24] Mingming He, Pascal Clausen, Ahmet Levent Taşel, Li Ma, Oliver Pilarski, Wenqi Xian, Laszlo Rikker, Xueming Yu, Ryan Burgert, Ning Yu, et al. Diffrelight: Diffusion-based facial performance relighting. In *SIGGRAPH Asia 2024 Conference Papers*, pages 1–12, 2024. **4**
- [25] Jonathan Ho, Ajay Jain, and Pieter Abbeel. Denoising diffusion probabilistic models. *Advances in Neural Information Processing Systems*, 33:6840–6851, 2020. **4, 6, 19**
- [26] Jonathan Ho, Chitwan Saharia, William Chan, David J Fleet, Mohammad Norouzi, and Tim Salimans. Cascaded diffusion models for high fidelity image generation. *J. Mach. Learn. Res.*, 23:47–1, 2022. **19**
- [27] Jonathan Ho and Tim Salimans. Classifier-free diffusion guidance. *arXiv:2207.12598*, 2022. **19**
- [28] Andrew Hou, Michel Sarkis, Ning Bi, Yiyong Tong, and Xiaoming Liu. Face relighting with geometrically consistent shadows. In *Proceedings of the IEEE/CVF Conference on Computer Vision and Pattern Recognition*, pages 4217–4226, 2022. **1, 2, 3, 7, 8, 10, 11, 18, 20**
- [29] Andrew Hou, Ze Zhang, Michel Sarkis, Ning Bi, Yiyong Tong, and Xiaoming Liu. Towards high fidelity face relighting with realistic shadows. In *Proceedings of the IEEE/CVF Conference on Computer Vision and Pattern Recognition*, pages 14719–14728, 2021. **1, 2, 3, 8, 10, 11, 20**
- [30] Luo Jiang, Juyong Zhang, Bailin Deng, Hao Li, and Ligang Liu. 3d face reconstruction with geometry details from a single image. *IEEE Transactions on Image Processing*, 27(10):4756–4770, 2018. **19**
- [31] Haian Jin, Yuan Li, Fujun Luan, Yuanbo Xiangli, Sai Bi, Kai Zhang, Zexiang Xu, Jin Sun, and Noah Snavely. Neural gaffer: Relighting any object via diffusion. In *Advances in Neural Information Processing Systems*, 2024. **3, 4, 10, 11, 12, 20**
- [32] Tero Karras, Samuli Laine, and Timo Aila. A style-based generator architecture for generative adversarial networks. In *Proceedings of the IEEE/CVF conference on computer vision and pattern recognition*, 2019. **4, 9, 11, 18, 24, 26, 27, 28, 29, 30, 31, 32, 33, 34, 35, 36, 43**
- [33] Zhanghan Ke, Chunyi Sun, Lei Zhu, Ke Xu, and Rynson W.H. Lau. Harmonizer: Learning to perform white-box image and video harmonization. In *European Conference on Computer Vision*, 2022. **4**
- [34] Hoon Kim, Minje Jang, Wonjun Yoon, Jisoo Lee, Donghyun Na, and Sanghyun Woo. Switchlight: Co-design of physics-driven architecture and pre-training framework for human portrait relighting, 2024. **1, 3, 4, 8, 19, 20, 21, 23**
- [35] Ha A Le and Ioannis A Kakadiaris. Illumination-invariant face recognition with deep relit face images. In *2019 IEEE Winter Conference on Applications of Computer Vision (WACV)*. IEEE, 2019. **1, 3**
- [36] Tianye Li, Timo Bolkart, Michael J. Black, Hao Li, and Javier Romero. Learning a model of facial shape and expression from 4D scans. *ACM Transactions on Graphics, (Proc. SIGGRAPH Asia)*, 2017. **5, 19**
- [37] Yijun Li, Ming-Yu Liu, Xueting Li, Ming-Hsuan Yang, and Jan Kautz. A closed-form solution to photorealistic image stylization. In *Proceedings of the European Conference on Computer Vision (ECCV)*, 2018. **4**
- [38] Yue Li, Liqian Ma, Haoqiang Fan, and Kenny Mitchell. Feature-preserving detailed 3d face reconstruction from a single image. In *Proceedings of the 15th ACM SIGGRAPH European Conference on Visual Media Production*, pages 1–9, 2018. **19**
- [39] Han Lin, Jaemin Cho, Abhay Zala, and Mohit Bansal. Ctrl-adapter: An efficient and versatile framework for adapting diverse controls to any diffusion model, 2024. **13**
- [40] Jingtuo Liu, Yafeng Deng, Tao Bai, Zhengping Wei, and Chang Huang. Targeting ultimate accuracy: Face recognition via deep embedding. *arXiv:1506.07310*, 2015. **19**
- [41] Cheng Lu, Yuhao Zhou, Fan Bao, Jianfei Chen, Chongxuan Li, and Jun Zhu. Dpm-solver: A fast ode solver for diffusion probabilistic model sampling in around 10 steps. *Advances in Neural Information Processing Systems*, 35:5775–5787, 2022. **4, 8**
- [42] Cheng Lu, Yuhao Zhou, Fan Bao, Jianfei Chen, Chongxuan Li, and Jun Zhu. Dpm-solver++: Fast solver for guided sampling of diffusion probabilistic models. *arXiv:2211.01095*, 2022. **4, 8**
- [43] Fujun Luan, Sylvain Paris, Eli Shechtman, and Kavita Bala. Deep photo style transfer. In *Proceedings of the IEEE conference on computer vision and pattern recognition*, pages 4990–4998, 2017. **4**
- [44] BR Mallikarjun, Ayush Tewari, Abdallah Dib, Tim Weyrich, Bernd Bickel, Hans Peter Seidel, Hanspeter Pfister, Wojciech Matusik, Louis Chevallier, Mohamed A Elgharib, et al. Photoapp: Photorealistic appearance editing of head portraits. *ACM Transactions on Graphics*, 2021. **4**
- [45] Iacopo Masi, Anh Tuấn Trần, Tal Hassner, Gozde Sahin, and Gérard Medioni. Face-specific data augmentation for unconstrained face recognition. *International Journal of Computer Vision*, 127, 2019. **19**
- [46] Yiqun Mei, Yu Zeng, He Zhang, Zhixin Shu, Xuaner Zhang, Sai Bi, Jianming Zhang, HyunJoon Jung, and Vishal M Patel. Holo-relighting: Controllable volumetric portrait relighting from a single image. *arXiv:2403.09632*, 2024. **1, 3, 4, 8, 19, 20, 21, 22**
- [47] Chenlin Meng, Yutong He, Yang Song, Jiaming Song, Jiajun Wu, Jun-Yan Zhu, and Stefano Ermon. Sdedit: Guided image synthesis and editing with stochastic differential equations. In *International Conference on Learning Representations*, 2021. **19**
- [48] Thomas Nestmeyer, Jean-François Lalonde, Iain Matthews, and Andreas Lehrmann. Learning physics-guided face relighting under directional light. In *Proceedings of the IEEE/CVF Conference on Computer Vision and Pattern Recognition*, pages 5124–5133, 2020. **1, 3, 8, 10, 20**
- [49] Alex Nichol, Prafulla Dhariwal, Aditya Ramesh, Pranav Shyam, Pamela Mishkin, Bob McGrew, Ilya Sutskever, and Mark Chen. Glide: Towards photorealistic image generation and editing with text-guided diffusion models. *arXiv:2112.10741*, 2021. **5, 19**
- [50] Kushagra Pandey, Avideep Mukherjee, Piyush Rai, and Abhishek Kumar. Vaes meet diffusion models: Efficient and high-fidelity generation. In *NeurIPS 2021 Workshop on Deep Generative Models and Downstream Applications*, 2021. **19**
- [51] Rohit Pandey, Sergio Orts Escolano, Chloe Legendre, Christian Haene, Sofien Bouaziz, Christoph Rhemann, Paul Debevec, and Sean Fanello. Total relighting: learning to relight portraits for background replacement. *ACM Transactions on Graphics (TOG)*, 40(4):1–21, 2021. **1, 3, 8, 10, 11, 20**
- [52] Foivos Paraperas Papantoniou, Alexandros Lattas, Stylianos Moschoglou, and Stefanos Zafeiriou. Relightify: Relightable 3d faces from a single image via diffusion models. In *Proceedings of the IEEE/CVF International Conference on Computer Vision*, 2023. **3**
- [53] Omkar M Parkhi, Andrea Vedaldi, and Andrew Zisserman. Deep face recognition. 2015. **19**
- [54] Puntawat Ponglertrnakorn, Nontawat Tritrong, and Supasorn Suwajanakorn. Difareli: Diffusion face relighting. *arXiv:2304.09479*, 2023. **2, 3, 6, 7, 8, 11, 12, 20**
- [55] Ben Poole, Ajay Jain, Jonathan T Barron, and Ben Mildenhall. Dreamfusion: Text-to-3d using 2d diffusion. *arXiv:2209.14988*, 2022. **19**
- [56] Konpat Preechakul, Nattanat Chatthee, Suttisak Wizadwongsa, and Supasorn Suwajanakorn. Diffusion autoencoders: Toward a meaningful and decodable representation. In *Proceedings of the IEEE/CVF Conference on Computer Vision and Pattern Recognition*, pages 10619–10629, 2022. **2, 4, 5, 6, 7, 19, 21**
- [57] Alec Radford, Jong Wook Kim, Chris Hallacy, Aditya Ramesh, Gabriel Goh, Sandhini Agarwal, Girish Sastry, Amanda Askell, Pamela Mishkin, Jack Clark, et al. Learning transferable visual models from natural language supervision. In *International Conference on Machine Learning*, pages 8748–8763. PMLR, 2021. **19**
- [58] Colin Raffel, Noam Shazeer, Adam Roberts, Katherine Lee, Sharan Narang, Michael Matena, Yanqi Zhou, Wei Li, and Peter J Liu. Exploring the limits of transfer learning with a unified text-to-text transformer. *The Journal of Machine Learning Research*, 21(1):5485–5551, 2020. **19**
- [59] Aditya Ramesh, Prafulla Dhariwal, Alex Nichol, Casey Chu, and Mark Chen. Hierarchical text-conditional image generation with clip latents. *arXiv:2204.06125*, 2022. **19**
- [60] Anurag Ranjan, Kwang Moo Yi, Jen-Hao Rick Chang, and Oncel Tuzel. Facelit: Neural 3d relightable faces, 2023. **4**
- [61] Mengwei Ren, Wei Xiong, Jae Shin Yoon, Zhixin Shu, Jianming Zhang, HyunJoon Jung, Guido Gerig, and He Zhang. Relightful harmonization: Lighting-aware portrait background replacement, 2023. **3, 4, 8**
- [62] Elad Richardson, Yuval Alaluf, Or Patashnik, Yotam Nitzan, Yaniv Azar, Stav Shapiro, and Daniel Cohen-Or. Encoding in style: a stylegan encoder for image-to-image translation. In *Proceedings of the IEEE/CVF conference on computer vision and pattern recognition*, 2021. **4**
- [63] Daniel Roich, Ron Mokady, Amit H Bermano, and Daniel Cohen-Or. Pivotal tuning for latent-based editing of real images. *ACM Transactions on Graphics (TOG)*, 42(1):1–13, 2022. **4**
- [64] Robin Rombach, Andreas Blattmann, Dominik Lorenz, Patrick Esser,

- and Björn Ommer. High-resolution image synthesis with latent diffusion models, 2021. 5, 13
- [65] Robin Rombach, Andreas Blattmann, Dominik Lorenz, Patrick Esser, and Björn Ommer. High-resolution image synthesis with latent diffusion models. In *Proceedings of the IEEE/CVF Conference on Computer Vision and Pattern Recognition*, pages 10684–10695, 2022. 19
- [66] Nataniel Ruiz, Yuanzhen Li, Varun Jampani, Yael Pritch, Michael Rubinstein, and Kfir Aberman. Dreambooth: Fine tuning text-to-image diffusion models for subject-driven generation. *arXiv:2208.12242*, 2022. 19
- [67] Chitwan Saharia, William Chan, Huiwen Chang, Chris Lee, Jonathan Ho, Tim Salimans, David Fleet, and Mohammad Norouzi. Palette: Image-to-image diffusion models. In *ACM SIGGRAPH 2022 Conference Proceedings*, pages 1–10, 2022. 19
- [68] Chitwan Saharia, William Chan, Saurabh Saxena, Lala Li, Jay Whang, Emily Denton, Seyed Kamyar Seyed Ghasemipour, Burcu Karagol Ayan, S Sara Mahdavi, Rapha Gontijo Lopes, et al. Photorealistic text-to-image diffusion models with deep language understanding. *arXiv:2205.11487*, 2022. 19
- [69] Shunsuke Saito, Gabriel Schwartz, Tomas Simon, Junxuan Li, and Giljoo Nam. Relightable gaussian codec avatars. In *Proceedings of the IEEE/CVF Conference on Computer Vision and Pattern Recognition*, pages 130–141, 2024. 4
- [70] Axel Sauer, Dominik Lorenz, Andreas Blattmann, and Robin Rombach. Adversarial diffusion distillation. *arXiv:2311.17042*, 2023. 3, 4
- [71] Florian Schroff, Dmitry Kalenichenko, and James Philbin. Facenet: A unified embedding for face recognition and clustering. In *Proceedings of the IEEE conference on computer vision and pattern recognition*, pages 815–823, 2015. 19
- [72] Soumyadip Sengupta, Angjoo Kanazawa, Carlos D Castillo, and David W Jacobs. Sfsnet: Learning shape, reflectance and illuminance of faces in the wild. In *Proceedings of the IEEE conference on computer vision and pattern recognition*, 2018. 1, 3, 8, 19, 20
- [73] YiChang Shih, Sylvain Paris, Connelly Barnes, William T Freeman, and Frédo Durand. Style transfer for headshot portraits. 2014. 4
- [74] Zhixin Shu, Sunil Hadap, Eli Shechtman, Kalyan Sunkavalli, Sylvain Paris, and Dimitris Samaras. Portrait lighting transfer using a mass transport approach. *ACM Transactions on Graphics (TOG)*, 2017. 4, 19
- [75] Zhixin Shu, Ersin Yumer, Sunil Hadap, Kalyan Sunkavalli, Eli Shechtman, and Dimitris Samaras. Neural face editing with intrinsic image disentangling. In *Proceedings of the IEEE conference on computer vision and pattern recognition*, pages 5541–5550, 2017. 1, 3
- [76] Abhishek Sinha, Jiaming Song, Chenlin Meng, and Stefano Ermon. D2c: Diffusion-decoding models for few-shot conditional generation. *Advances in Neural Information Processing Systems*, 34, 2021. 19
- [77] Jascha Sohl-Dickstein, Eric Weiss, Niru Maheswaranathan, and Surya Ganguli. Deep unsupervised learning using nonequilibrium thermodynamics. In Francis Bach and David Blei, editors, *Proceedings of the 32nd International Conference on Machine Learning*, Proceedings of Machine Learning Research, pages 2256–2265. PMLR, 2015. 4, 19
- [78] Jiaming Song, Chenlin Meng, and Stefano Ermon. Denoising diffusion implicit models. In *International Conference on Learning Representations*, 2021. 2, 4, 6
- [79] Yang Song, Prafulla Dhariwal, Mark Chen, and Ilya Sutskever. Consistency models. *arXiv:2303.01469*, 2023. 3, 4
- [80] Yang Song and Stefano Ermon. Generative modeling by estimating gradients of the data distribution. In H. Wallach, H. Larochelle, A. Beygelzimer, F. d’Alché-Buc, E. Fox, and R. Garnett, editors, *Advances in Neural Information Processing Systems*, volume 32. Curran Associates, Inc., 2019. 4, 19
- [81] Tiancheng Sun, Jonathan T Barron, Yun-Ta Tsai, Zexiang Xu, Xueming Yu, Graham Fyffe, Christoph Rhemann, Jay Busch, Paul E Debevec, and Ravi Ramamoorthi. Single image portrait relighting. *ACM Trans. Graph.*, 38(4):79–1, 2019. 3, 8, 20
- [82] Yaniv Taigman, Ming Yang, Marc’Aurelio Ranzato, and Lior Wolf. Deepface: Closing the gap to human-level performance in face verification. In *Proceedings of the IEEE conference on computer vision and pattern recognition*, pages 1701–1708, 2014. 19
- [83] Ayush Tewari, Mohamed Elgharib, Florian Bernard, Hans-Peter Seidel, Patrick Pérez, Michael Zollhöfer, and Christian Theobalt. Pie: Portrait image embedding for semantic control. *ACM Transactions on Graphics (TOG)*, 39(6):1–14, 2020. 4
- [84] Ayush Tewari, Mohamed Elgharib, Gaurav Bharaj, Florian Bernard, Hans-Peter Seidel, Patrick Pérez, Michael Zollhofer, and Christian Theobalt. Stylerig: Rigging stylegan for 3d control over portrait images. In *Proceedings of the IEEE/CVF Conference on Computer Vision and Pattern Recognition*, pages 6142–6151, 2020. 4
- [85] Ayush Tewari, Tae-Hyun Oh, Tim Weyrich, Bernd Bickel, Hans-Peter Seidel, Hanspeter Pfister, Wojciech Matusik, Mohamed Elgharib, Christian Theobalt, et al. Monocular reconstruction of neural face reflectance fields. In *Proceedings of the IEEE/CVF Conference on Computer Vision and Pattern Recognition*, pages 4791–4800, 2021. 3
- [86] Ashish Vaswani, Noam Shazeer, Niki Parmar, Jakob Uszkoreit, Llion Jones, Aidan N Gomez, Łukasz Kaiser, and Illia Polosukhin. Attention is all you need. *Advances in neural information processing systems*. 19
- [87] Ke Wang, Michaël Gharbi, He Zhang, Zhihao Xia, and Eli Shechtman. Semi-supervised parametric real-world image harmonization. In *Proceedings of the IEEE/CVF Conference on Computer Vision and Pattern Recognition*, pages 5927–5936, 2023. 4
- [88] Mei Wang and Weihong Deng. Deep face recognition: A survey. *Neurocomputing*, 429:215–244, 2021. 19
- [89] Yang Wang, Lei Zhang, Zicheng Liu, Gang Hua, Zhen Wen, Zhengyou Zhang, and Dimitris Samaras. Face relighting from a single image under arbitrary unknown lighting conditions. *IEEE Transactions on Pattern Analysis and Machine Intelligence*, 31(11):1968–1984, 2008. 1, 3
- [90] Zhibo Wang, Xin Yu, Ming Lu, Quan Wang, Chen Qian, and Feng Xu. Single image portrait relighting via explicit multiple reflectance channel modeling. *ACM Transactions on Graphics (TOG)*, 39(6), 2020. 3
- [91] Daniel Watson, William Chan, Jonathan Ho, and Mohammad Norouzi. Learning fast samplers for diffusion models by differentiating through sample quality. In *International Conference on Learning Representations*, 2021. 4
- [92] Andreas Wenger, Andrew Gardner, Chris Tchou, Jonas Unger, Tim Hawkins, and Paul Debevec. Performance relighting and reflectance transformation with time-multiplexed illumination. *ACM Transactions on Graphics (TOG)*, 24(3):756–764, 2005. 3
- [93] Yuxin Wu and Kaiming He. Group normalization. In *Proceedings of the European conference on computer vision (ECCV)*, pages 3–19, 2018. 5, 6
- [94] Jiaxin Xie, Hao Ouyang, Jingtan Piao, Chenyang Lei, and Qifeng Chen. High-fidelity 3d gan inversion by pseudo-multi-view optimization. In *Proceedings of the IEEE/CVF Conference on Computer Vision and Pattern Recognition*, pages 321–331, 2023. 4
- [95] Yanwu Xu, Yang Zhao, Zhisheng Xiao, and Tingbo Hou. Ufogen: You forward once large scale text-to-image generation via diffusion gans. *arXiv:2311.09257*, 2023. 3, 4
- [96] Yu-Ying Yeh, Koki Nagano, Sameh Khamis, Jan Kautz, Ming-Yu Liu, and Ting-Chun Wang. Learning to relight portrait images via a virtual light stage and synthetic-to-real adaptation. *ACM Transactions on Graphics (TOG)*, 41(6):1–21, 2022. 1, 3
- [97] Changqian Yu, Jingbo Wang, Chao Peng, Changxin Gao, Gang Yu, and Nong Sang. Bisenet: Bilateral segmentation network for real-time semantic segmentation. In *Proceedings of the European conference on computer vision (ECCV)*, pages 325–341, 2018. 3, 5, 7, 8
- [98] Chong Zeng, Yue Dong, Pieter Peers, Youkang Kong, Hongzhi Wu, and Xin Tong. Dilightnet: Fine-grained lighting control for diffusion-based image generation. In *ACM SIGGRAPH 2024 Conference Papers*, 2024. 4
- [99] Lvmin Zhang, Anyi Rao, and Maneesh Agrawala. Adding conditional control to text-to-image diffusion models. In *Proceedings of the IEEE/CVF International Conference on Computer Vision*, pages 3836–3847, 2023. 2, 12, 19
- [100] Lvmin Zhang, Anyi Rao, and Maneesh Agrawala. Ic-light github page, 2024. 3, 4, 8, 10, 11, 20, 45
- [101] Richard Zhang, Phillip Isola, Alexei A Efros, Eli Shechtman, and Oliver Wang. The unreasonable effectiveness of deep features as a perceptual metric. In *Proceedings of the IEEE conference on computer vision and pattern recognition*, pages 586–595, 2018. 8
- [102] Xuaner Zhang, Jonathan T Barron, Yun-Ta Tsai, Rohit Pandey, Xiuming Zhang, Ren Ng, and David E Jacobs. Portrait shadow manipulation. *ACM Transactions on Graphics (TOG)*, 2020. 19
- [103] Yuxuan Zhang, Yirui Yuan, Yiren Song, Haofan Wang, and Jiaming Liu. Easycontrol: Adding efficient and flexible control for diffusion transformer. *arXiv preprint arXiv:2503.07027*, 2025. 13
- [104] Wenliang Zhao, Lujia Bai, Yongming Rao, Jie Zhou, and Jiwen Lu. Unipc: A unified predictor-corrector framework for fast sampling of diffusion models. *arXiv:2302.04867*, 2023. 4, 8
- [105] Hao Zhou, Sunil Hadap, Kalyan Sunkavalli, and David W Jacobs. Deep single-image portrait relighting. In *Proceedings of the IEEE/CVF International Conference on Computer Vision*, 2019. 3, 8, 20



Puntawat Ponglertnapakorn is currently a Ph.D. student at the School of Information Science and Technology, Vidyasirimedhi Institute of Science and Technology (VISTEC), Thailand. He received the B.Eng. degree from Prince of Songkla University (PSU), Thailand, in 2018. His research interest is computer vision.



Nontawat Tritrong is currently a Ph.D. student at the School of Information Science and Technology, Vidyasirimedhi Institute of Science and Technology (VISTEC), Thailand. He received the B.Sc. degree from Suranaree University of Technology (SUT), Thailand, in 2019. His research interest is representation learning.



Supasorn Suwajanakorn received the B.Eng. degree from Cornell University, in 2011 and the Ph.D. degree from the University of Washington, in 2017. He is currently a lecturer with the school of Information Science and Technology (IST), Vidyasirimedhi Institute of Science and Technology (VISTEC), Thailand. His research interests lie in the intersection of computer vision, deep learning, and computer graphics.

Appendix for DiFaReli++: Diffusion Face Relighting with Consistent Cast Shadows

I. OVERVIEW

In this Appendix, we present:

- Section II: Implementation details.
- Section III: Network architectures.
- Section IV: 3D Face rendering.
- Section V: Additional related works.
- Section VI: Additional results.
- Section VII: Potential negative societal impacts.
- Section VIII: User interface for relighting user study.

II. IMPLEMENTATION DETAILS

A. Datasets

For all experiments in Section V-A, we trained our network on the FFHQ dataset [32], which consists of 70,000 aligned face images (60k for training and 10k for testing). We evaluated the relighting performance on Multi-PIE dataset [21], which contains 337 subjects captured under 19 flashes. In “self target lighting,” we use the same test set as [28], which contains pairs of images from the same person but in different lighting. For “target lighting from others,” we randomly pick 200 triplets of the input, target, and ground truth, where the target image is of a different person. For all ablation studies (Section V-E), to cap the computational resources, each ablated variation is trained on the FFHQ dataset at 128×128 resolution and evaluated on Multi-PIE dataset. For evaluation, we randomly pick 200 pairs, using the same policy as the “self target lighting,” from the disjoint set of other experiments in Section V-A.

B. Training and Inference

We normalize the training images to $[-1,1]$, and precompute their encodings from DECA, ArcFace, and our shadow estimator. We train our DDIM and Modulator using training hyperparameters in Table V.

128×128 resolution. We used four Nvidia RTX2080Tis for training and one Nvidia RTX2080Ti for testing. The training took around 1 day using batch size 32, and the inference took 101.38 ± 0.64 s per image.

256×256 resolution. We used four Nvidia V100s for training and one Nvidia RTX2080Ti for testing. The training took around 8 days using batch size 20, and the inference took 194.29 ± 9.17 s per image.

C. Improved DDIM sampling with mean-matching

We observe that when the input image contains background pixels with extreme intensities (e.g., too dark or too bright), the output tends to have a slight change in the overall brightness, most noticeable in the background (see Figure 44). This behavior also occurs with DDIM inversion that involves no relighting, i.e., when we reverse $\mathbf{x}_T = \text{DDIM}^{-1}(\mathbf{x}_0)$ and decode $\mathbf{x}'_0 = \text{DDIM}(\mathbf{x}_T)$ without modifying the light encoding, \mathbf{x}'_0 can look slightly different from \mathbf{x}_0 in terms of the overall brightness.

We found that we can correct the overall brightness with a simple, global brightness adjustment within DDIM’s generative process as follows. We first perform self-reconstruction by running DDIM’s reverse generative process starting from the input \mathbf{x}_0 to produce $\mathbf{x}_0, \mathbf{x}_1, \dots, \mathbf{x}_T$, then decoding back $\mathbf{x}'_T, \mathbf{x}'_{T-1}, \dots, \mathbf{x}'_0$, where $\mathbf{x}'_T = \mathbf{x}_T$ using Equation 4 in the main paper and its reverse. Then, our correction factor sequence, $\mu_0, \mu_1, \dots, \mu_T$, is computed by taking the difference between the mean pixel values of \mathbf{x} and \mathbf{x}' :

$$\mu_t = \text{mean}(\mathbf{x}'_t) - \text{mean}(\mathbf{x}_t). \quad (7)$$

We compute the mean separately for each RGB channel and compute this correction sequence *once* for each input image. Then, during relighting, we add μ_t to the generative process conditioned on the modified feature vector, starting from \mathbf{x}_T . That is, we use the reverse of Equation 4 in the main paper to first produce \mathbf{x}_{T-1} from \mathbf{x}_T , and add μ_{T-1} to it: $\mathbf{x}_{T-1} \leftarrow \mathbf{x}_{T-1} + \mu_{T-1}$. Then, we continue the process until we obtain the relit output at $t = 0$.

III. NETWORK ARCHITECTURES

A. Conditional DDIM & Modulator

Our conditional DDIM architecture is based on Dhariwal et al. [12], with two main differences: (1) the output of each residual block in the first half of the UNet is modulated by the signal from the Modulator network, and (2) we use our own version of adaptive group normalization. The Modulator shares the same architecture and hyperparameters as the first half of DDIM’s UNet but does not share weights. Each residual block in the first half of the network uses both spatial and non-spatial conditioning (Figure 16), while those in the second half use only non-spatial conditioning.

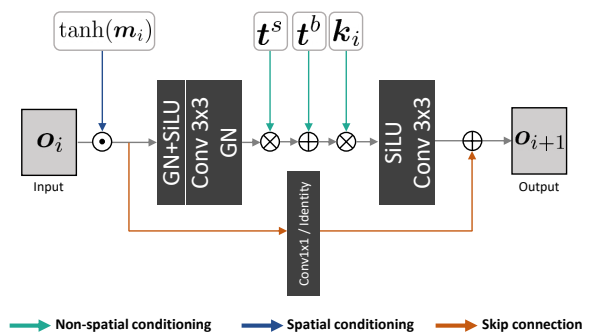


Fig. 16: Diagram of one of the residual blocks inside the first half of our conditional DDIM.

B. Non-spatial encoding

The concatenation of $(\mathbf{s}, \text{cam}, \boldsymbol{\xi}, c)$ is passed through 3-layer MLPs (Figure 17). For each MLP_i, we use fixed-dimension hidden layers $\mathbf{k}_i^1, \mathbf{k}_i^2 \in \mathbb{R}^{512}$, while the dimension of each \mathbf{k}_i depends on the channel dimension of each residual block.

TABLE V: Our conditional DDIM’s configuration is based on the architecture of [12].

Parameter	FFHQ 128	FFHQ 256
Base channels	128	128
Channel multipliers	[1,1,2,3,4]	[1,1,2,2,4,4]
Attention resolution	[16, 8]	[16, 8]
Batch size	32	20
Image trained	1.6M	1.7M
Diffusion step		1000
Learning rate		1e-4
Weight decay		-
Noise scheduler		Linear
Optimizer		AdamW

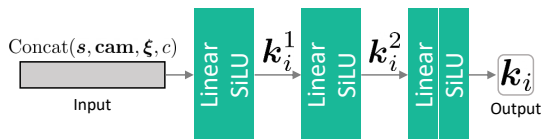


Fig. 17: Diagram of one of the 3-layer MLPs in the non-spatial conditioning branch.

C. ControlNet implementation for conditioning mechanism alternatives ablation (Section V-E3)

We follow the official implementations of ControlNet and cross-attention provided in the [GitHub repository](#) [99], with slight modifications. For all settings in Table IV, we use the same hyperparameters (e.g., base channels, channel multipliers, and attention resolutions) as our conditional DDIM (see Table V). For setting b) CN + DiFaReli++, we apply our non-spatial conditioning to ControlNet by injecting the non-spatial vector through AdaGN within each ResNet block (similar to DiffAE [56]), instead of through the cross-attention layer. For setting c) CN-Mod, we remove only the initial zero-convolution block. And for setting d), we feed our non-spatial vector into the cross-attention layer.

IV. 3D FACE RENDERING

We compute the shading reference R used in the spatial conditioning by:

$$R_{i,j} = A \odot \sum_{k=1}^9 \mathbf{1}_k H_k(N_{i,j}), \quad (8)$$

where i, j denote pixel (i, j) in image space, $A = [0.7, 0.7, 0.7]$ is a constant gray albedo, $l_k \in \mathbb{R}^3$ is the k -th second-order spherical harmonic RGB coefficient predicted from DECA, $H_k : \mathbb{R}^3 \rightarrow \mathbb{R}$ is the k -th spherical harmonic basis function, $N_{i,j} \in \mathbb{R}^3$ is the normalized surface normal at pixel (i, j) .

V. ADDITIONAL RELATED WORKS

Conditional DDPMs. Diffusion models (DDPMs) [25] and scored-based models [77], [80] have been used to solve multiple conditional generation tasks [9], such as conditional image synthesis [12], [27], [76], [8], image-to-image translation [67], image super-resolution [26], [50], image segmentation [1], [4]

and image manipulation [56], [47]. Many recent approaches use cross-modal embeddings from popular language models [57], [86], [58] as conditions for diffusion models [59], [68], [65], [66], [49], [2], [55], [99], which enables general text-to-image generation and image manipulation. However, they lack the ability to precisely manipulate lighting attributes or directions. DiffAE [56] conditions a DDIM with a 1D latent vector that is learned to capture semantically meaningful information. Manipulating this novel latent vector allows manipulation of various semantic face attributions. Unlike DiffAE, which implicitly models semantic attributes via a learnable latent code, our method requires an explicit and interpretable light encoding, which can be controlled by the user.

Single-view 3D face modeling. Our work uses DECA [17] to estimate the 3D shape and spherical harmonic lighting information. Based on the pioneer work of Blanz and Vetter [6], DECA regresses the parameters of a FLAME model [36], which represents the face shape with three linear bases corresponding to the identity shape, pose, and expression, and further recovers person-specific details that can change with expression. Our work only uses the FLAME estimate from DECA without the additional facial details. Note that other 3D face modeling techniques, such as [11], [19], [30], [38], can also be used in our framework.

Face recognition model for deep face embedding. Our work leverages a face recognition model, ArcFace [10], to preserve the identity of the relit face. Most previous face recognition models are trained using softmax loss [82], [53], [45] and triplet loss [71], [40] (See [88] for a review.) However, they do not generalize well with open-set recognition and large scale recognition. ArcFace adopts Additive Angular Margin loss, which retains discriminativeness while avoiding the sampling problem of the triplet loss. Arcface also proposed a sub-center procedure, which helps improve the robustness of the embedding. Note again that other face embedding models, such as [82], [53], [45], [40], can also be used in our framework.

VI. ADDITIONAL RESULTS

In this section, we provide additional results:

- Table VI shows full statistics of Table 1 (Top, main paper) with standard errors, as well as more results from additional baselines [72], [102], [74].
- Figures 21 and 22 show qualitative results from the ablation study on alternative conditioning mechanisms (Section V-E3).
- Figure 23 shows qualitative results of the ablation study on light conditioning (Section V-E1).
- Figure 24 shows qualitative results of the ablation study on non-spatial conditioning (Section V-E2).
- Figure 13 shows qualitative results of the ablation study on background conditioning.
- Figure 25, 26, 27, 28, 29, 30, 31, 32 and 33 show additional qualitative results on the FFHQ dataset.
- Figures 19 and 20 show qualitative comparisons with two recent state-of-the-art methods, HoloRelighting [46] and SwitchLight [34].

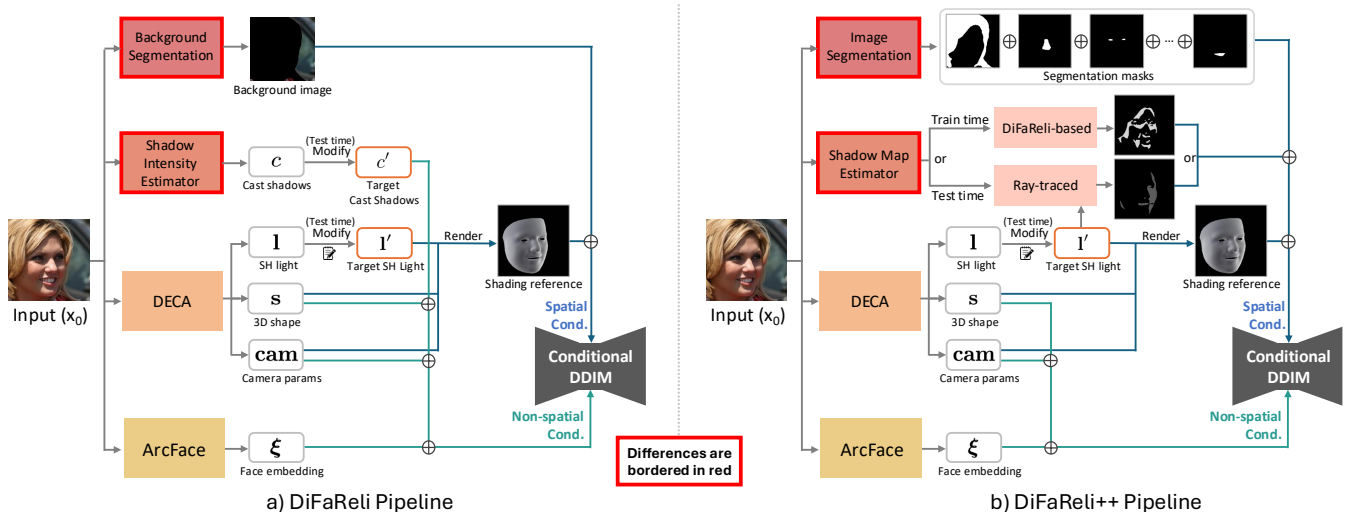


Fig. 18: **Comparison of DiFaReli and DiFaReli++ pipelines.** Differences are highlighted with red borders. Key changes are: 1) Background conditioning: replacing the background image with a concatenation of segmentation masks to enable relighting of non-facial parts. 2) Shadow estimator: using a shadow map with an encoded shadow scalar for improved consistency in cast shadows generation. 3) The cast shadow scalar c is not longer part of the non-spatial conditioning.

TABLE VI: **State-of-the-art comparison on Multi-PIE.** We report the means and standard errors. Our method outperforms all previous methods on all metrics with p-values < 0.001 .

Method	DDSIM↓		MSE↓		LPIPS↓	
	Mean	SE	Mean	SE	Mean	SE
SfSNet [72]	0.2918	0.0013	0.0961	0.0017	0.5222	0.0025
DPR [105]	0.1599	0.0019	0.0852	0.0018	0.2644	0.0028
SIPR [81]	0.1539	0.0015	0.0166	0.0004	0.2764	0.0025
Nestmayer et al. [48]	0.2226	0.0046	0.0588	0.0018	0.3795	0.0078
Pandey et al. [51]	0.0875	0.0007	0.0165	0.0003	0.2010	0.0022
Hou et al.(CVPR'21) [29]	0.1186	0.0013	0.0303	0.0006	0.2013	0.0023
Hou et al.(CVPR'22) [28]	0.0990	0.0013	0.0150	0.0004	0.1622	0.0017
Ding et al. (CVPR'23) [13]	0.0870	0.0009	0.0098	0.0002	0.2098	0.0014
Zhang et al. (IC-Light's github) [100]	0.1978	0.0015	0.0499	0.0017	0.1887	0.0063
Guo et al. (CVPR'25) [22]	0.1088	0.0015	0.0234	0.0006	0.1733	0.0018
Ours (DiFaReli [54])	0.0711	0.0011	0.0122	0.0005	0.1370	0.0020
Ours (DiFaReli++)	0.0604	0.0010	0.0090	0.0003	0.1043	0.0013
Ours (DiFaReli++_{ss})	0.0590	0.0009	0.0075	0.0002	0.1023	0.0013

- Figures 34 and 35 show qualitative comparisons with recent object relighting methods, Neural Gaffer [31].
- Figures 36, 37, 38, 39, 40, 41, 42 and 43 show qualitative comparisons on tuning the relighting hyperparameters for DiffusionRig [13] and Guo et al.[22].
- Figure 44 shows a qualitative comparison for the ablation study of the mean-matching algorithm (Section II-C).
- Figure 45 shows more qualitative results on cast shadow manipulation.

A. Additional results and comparison with concurrent relighting methods that use HDR environment map

In this section, we show additional qualitative results of Pandey et al. [51], as a supplement to Figure 6 from the main paper. We also compare our method with two concurrent works, HoloRelighting [46] and SwitchLight [34]. As none

of these methods [51], [46], [34] released their source code, and their datasets are proprietary, we requested the authors to test their algorithms on the standard Multi-PIE and FFHQ datasets. Only Pandey et al. [51] provided results generated by the authors themselves, including the estimated environment maps. For HoloRelighting [46] and SwitchLight [34], we cropped and ran our algorithm on the samples provided in their papers.

Figures 30, 31, 32, and 33 show additional subjects compared with Pandey et al. [51]. Our method produces more photorealistic results with synthesized cast shadows, whereas [51] tends to produce blurrier outputs with white area artifacts. For example, such artifacts are observable on the forehead of the first subject (Figure 33) and the third subject (Figure 30).

We provide a qualitative comparison with HoloRelighting in Figure 19 and SwitchLight in Figure 20. Compared to HoloRelighting [46], our method preserves finer details like

hair and teeth (first and third rows) and more effectively removes cast shadows from the input images (second rows). We also address the limitations discussed in SwitchLight [34], showing improved removal of hard cast shadows (first row) and preserving makeup from the input image (second row).

Despite these improvements, our relighting results might not perfectly match the target lighting, as our method relies on the DECA light estimator [16]. As shown in Figure 19 and 20, the estimated lighting from DECA fails to replicate the shading colors in the input images (e.g., yellow-tinted or greenish tones). We also suspect a discrepancy between the target lighting and the lighting conditions in our training set.

To test this, we performed a visual analysis of our failure cases, shown below each qualitative comparison in Figure 19 and 20. Each row shows the top eight closest lighting examples, retrieved by computing pixel-wise L1 distances between rendered sphere images from the FFHQ training set and the target lighting image. The spheres were rendered with estimated spherical harmonics (SH) from DECA [16], using the FFHQ training set as the retrieval set and the target lighting image (from [46], [34]) as the query. Areas outside the sphere were masked during computation. This analysis shows that the training set used to train DiFaReli++ does not contain similar yellow-tinted or greenish effects, even in the top closest lighting examples.

Although our method relies on this light estimator, it is designed to be flexible and can easily integrate with any state-of-the-art light estimator to address such cases. However, there are currently few publicly available light estimators, especially for portrait images, and this area of research remains under active development.

VII. POTENTIAL NEGATIVE SOCIETAL IMPACTS

Our method can be used for changing the lighting condition of an existing image and producing the so-called DeepFake, which can deceive human visual perception. Our manipulation process is based on conditional DDIM [12], and a study from [56], which uses the same architecture, shows that certain artifacts from DDIM can be currently detected using a CNN with about 92% accuracy. We developed our work with the intention of promoting positive and creative uses, and we do not condone any misuse of our work.

VIII. USER INTERFACE FOR RELIGHTING USER STUDY

Figure 50, 51, and 52 show the user interfaces used in our user studies, as detailed in Section V-C of the main paper. Each page contains 10 tasks, each with 2 questions (a total of 20 questions per page).

For each task, an input image is displayed along with the target lighting condition, with irrelevant areas masked out to help users focus on either the face region or the entire person. The order of results for each task is shuffled when displayed to each participant. Instructions and criteria for making selections are provided at the top of the page.

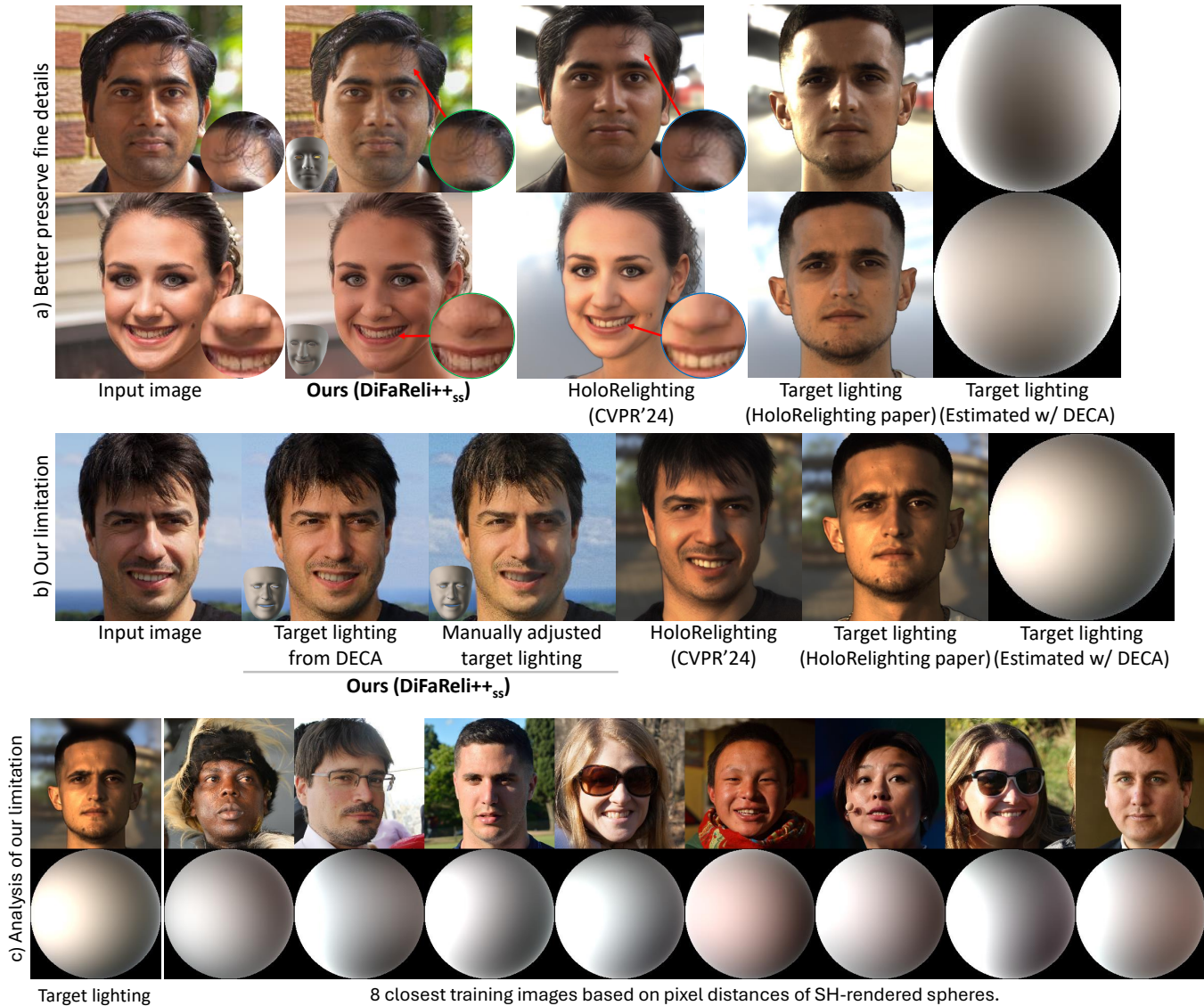


Fig. 19: **Comparison against HoloRelighting [46] and visual analysis of our limitations.** a) Our method better preserves fine details, such as hair and teeth, compared to HoloRelighting results, taken directly from their paper due to the lack of source code. Note that our target lighting was estimated using DECA [16] from the target image. b) The overall lighting in our result lacks the strong orange shading present in the target shading. c) To analyze this issue, we retrieve the 8 closest training images based on SH coefficient distances, revealing that none of them has the orange-tinted shading. This suggests that the current limitation may stem from the lack of such lighting conditions in our FFHQ training data. Nonetheless, our pipeline can readily be trained on additional 2D training images, including extreme lighting conditions, without requiring ground truth.

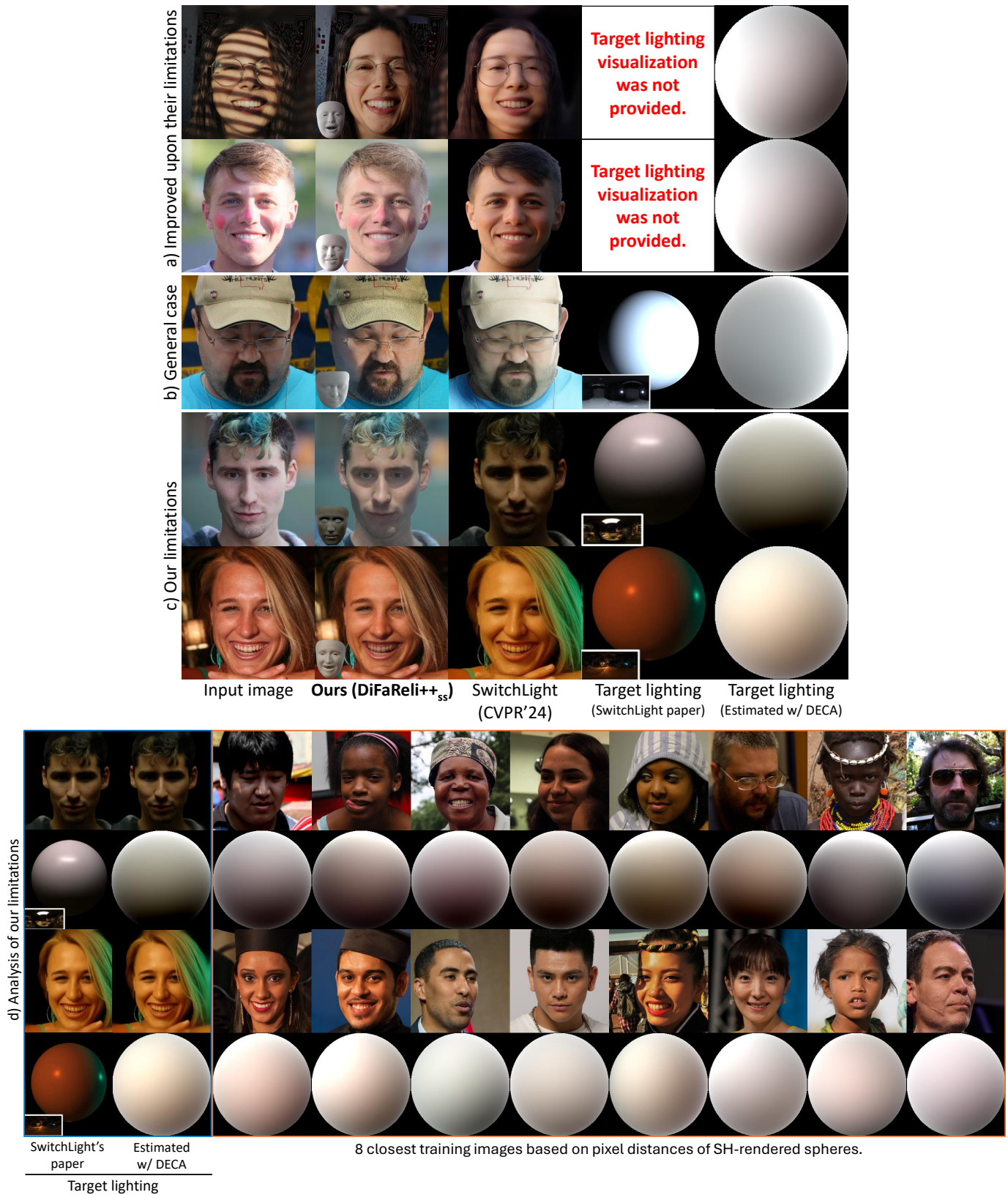


Fig. 20: **Comparison against SwitchLight [34] and visual analysis of our limitations.** SwitchLight’s results were taken directly from their paper due to the lack of source code. Our method addresses SwitchLight’s limitations: a) our method effectively removes hard cast shadows and better preserves makeup details, and b) produces sharper details. c) Our results appear less consistent with the target lighting, lacking the sufficiently dark lighting or the green shading. As in Figure 19, we retrieve the closest training images for these cases. The results show that our light estimator, DECA, struggles with skin-tone and light ambiguity, retrieving dark-skinned individuals instead of images with dark lighting, resulting in a biased training set. Additionally, the retrieved set lacks green lighting, as seen in the test image of the woman, which may explain our difficulties. This can be addressed by scaling up the training set, which only requires 2D images.

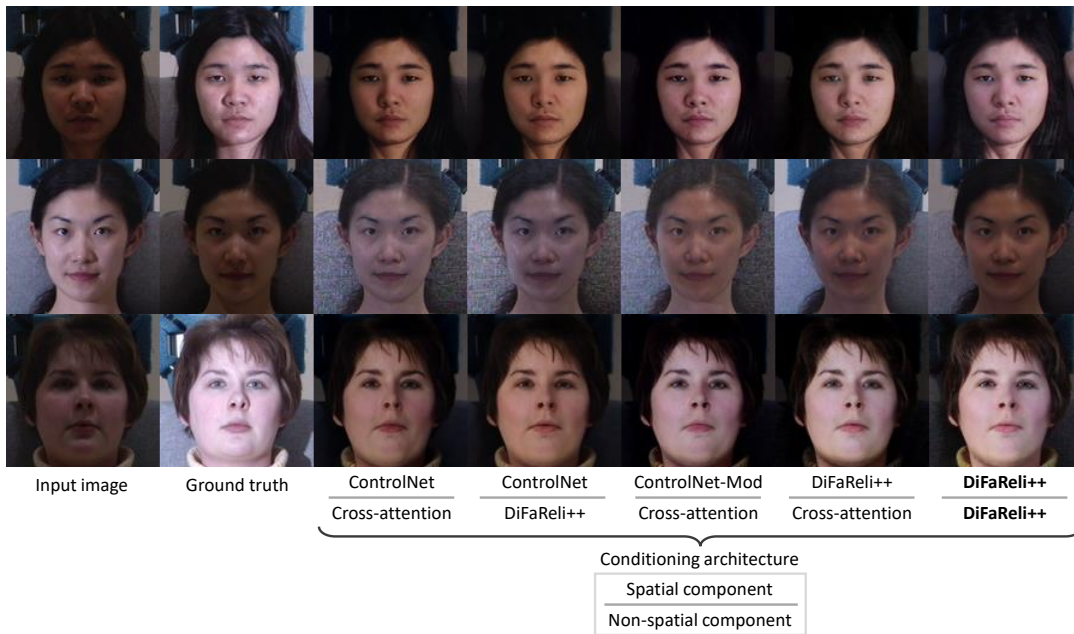


Fig. 21: Ablation study of the conditioning mechanisms on MultiPIE [21] (Section V-E3 in the main paper).



Fig. 22: Ablation study of the conditioning mechanisms on FFHQ [32] (Section V-E3 in the main paper).

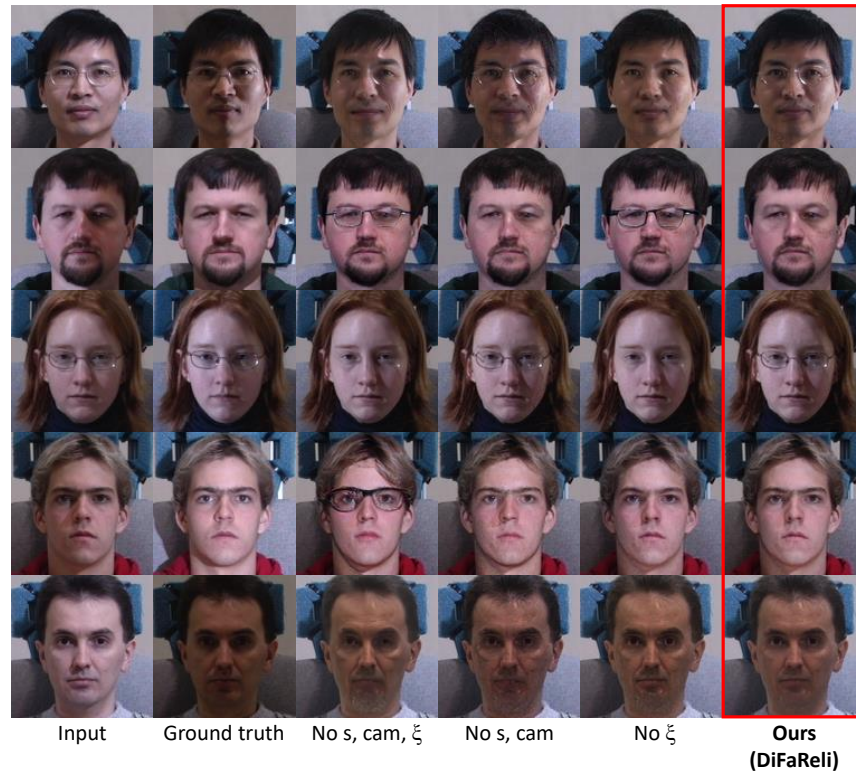


Fig. 23: Ablation study of the light conditioning (Section V-E1 in Appendix).

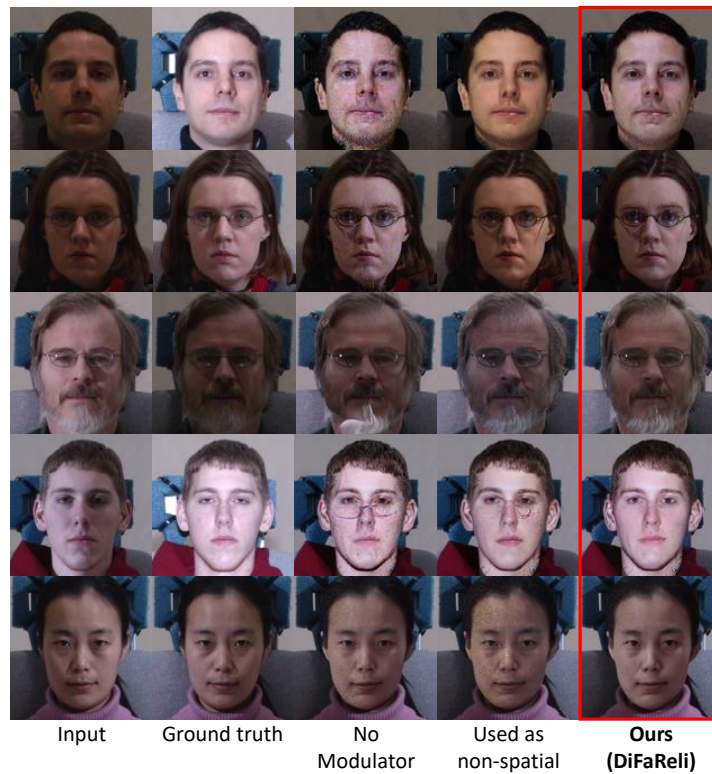


Fig. 24: Ablation study of the non-spatial conditioning variable (Section V-E2 in Appendix).

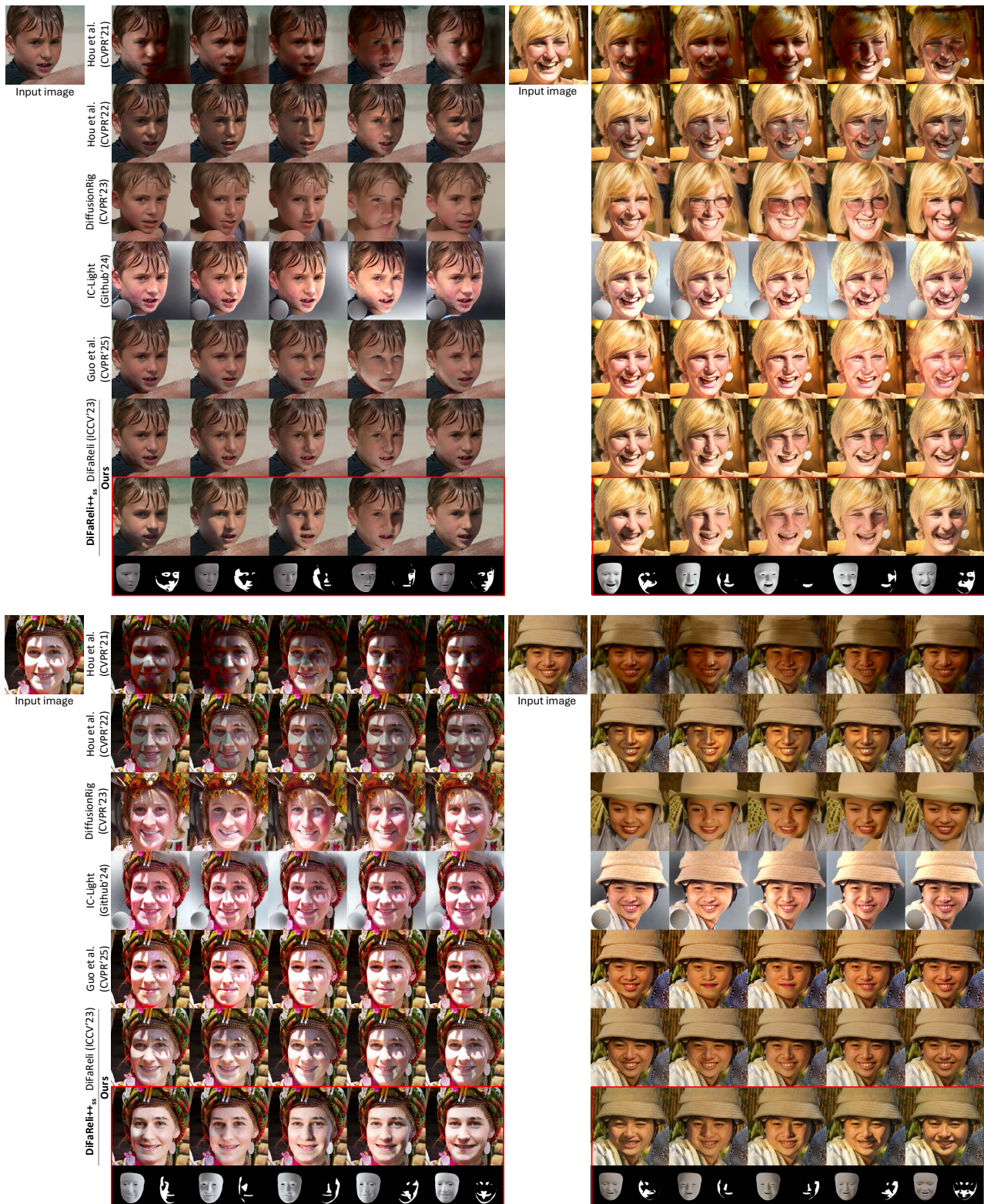


Fig. 25: Relit results under rotating light around the forward axis (roll) on the FFHQ test set [32].

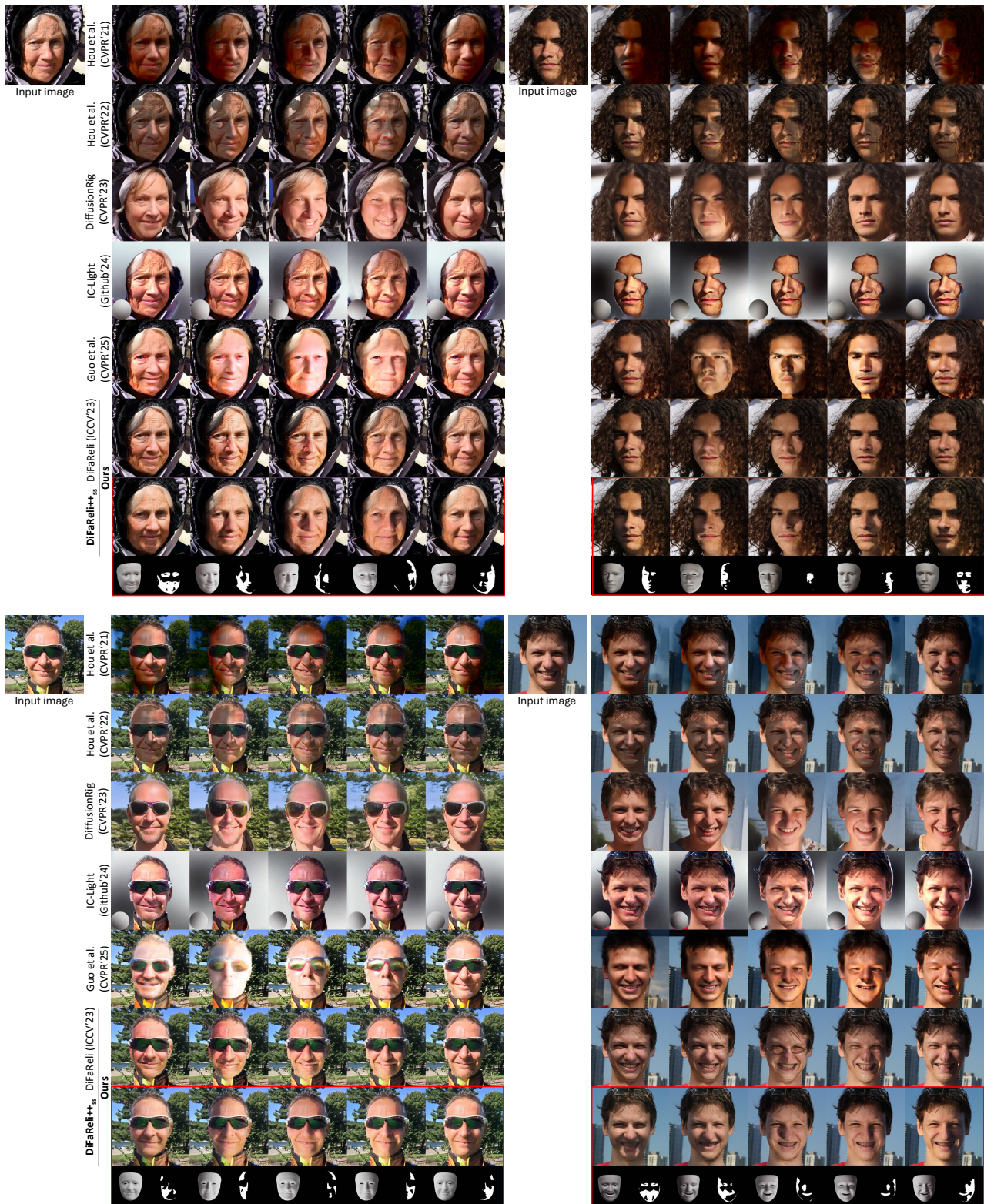


Fig. 26: Relit results under rotating light around the forward axis (roll) on the FFHQ test set [32].



Fig. 27: Relit results under rotating light around the forward axis (roll) on the FFHQ test set [32].

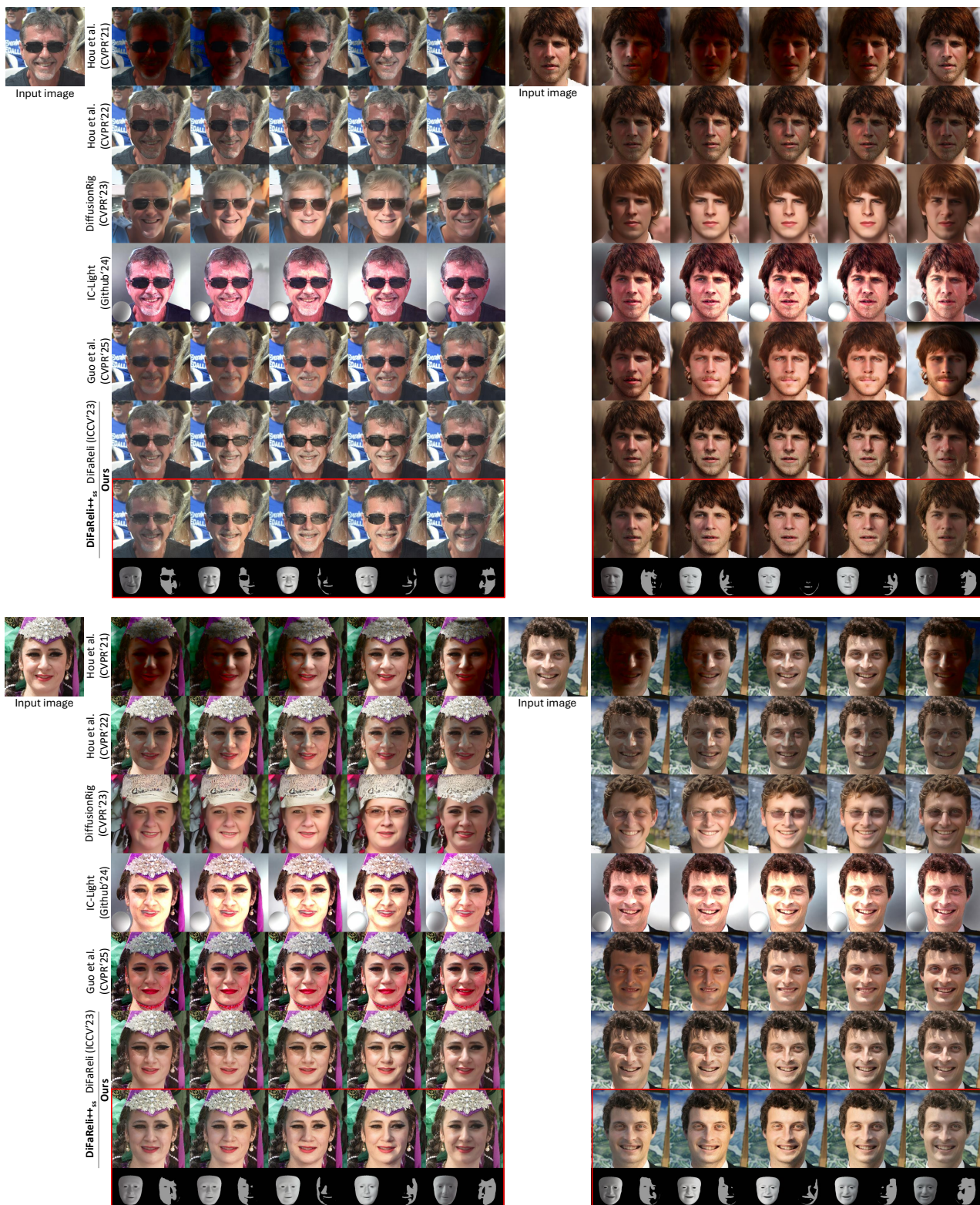


Fig. 28: Relit results under rotating light around the up axis (yaw) on the FFHQ test set [32].

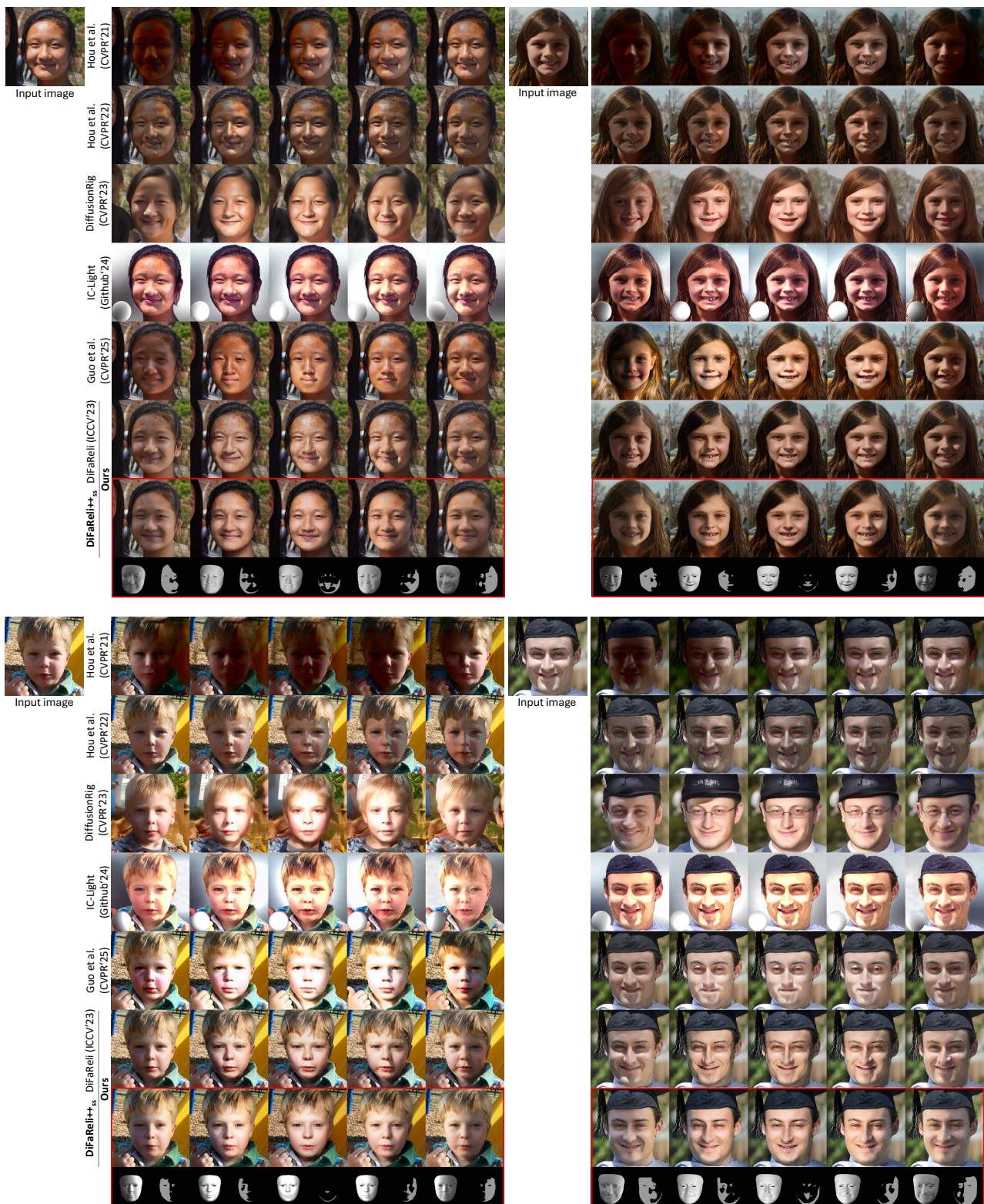


Fig. 29: Relit results under rotating light around the up axis (yaw) on the FFHQ test set [32].



Fig. 30: Relit results under a given target lighting image on the FFHQ test set [32].



Fig. 31: Relit results under a given target lighting image on the FFHQ test set [32].

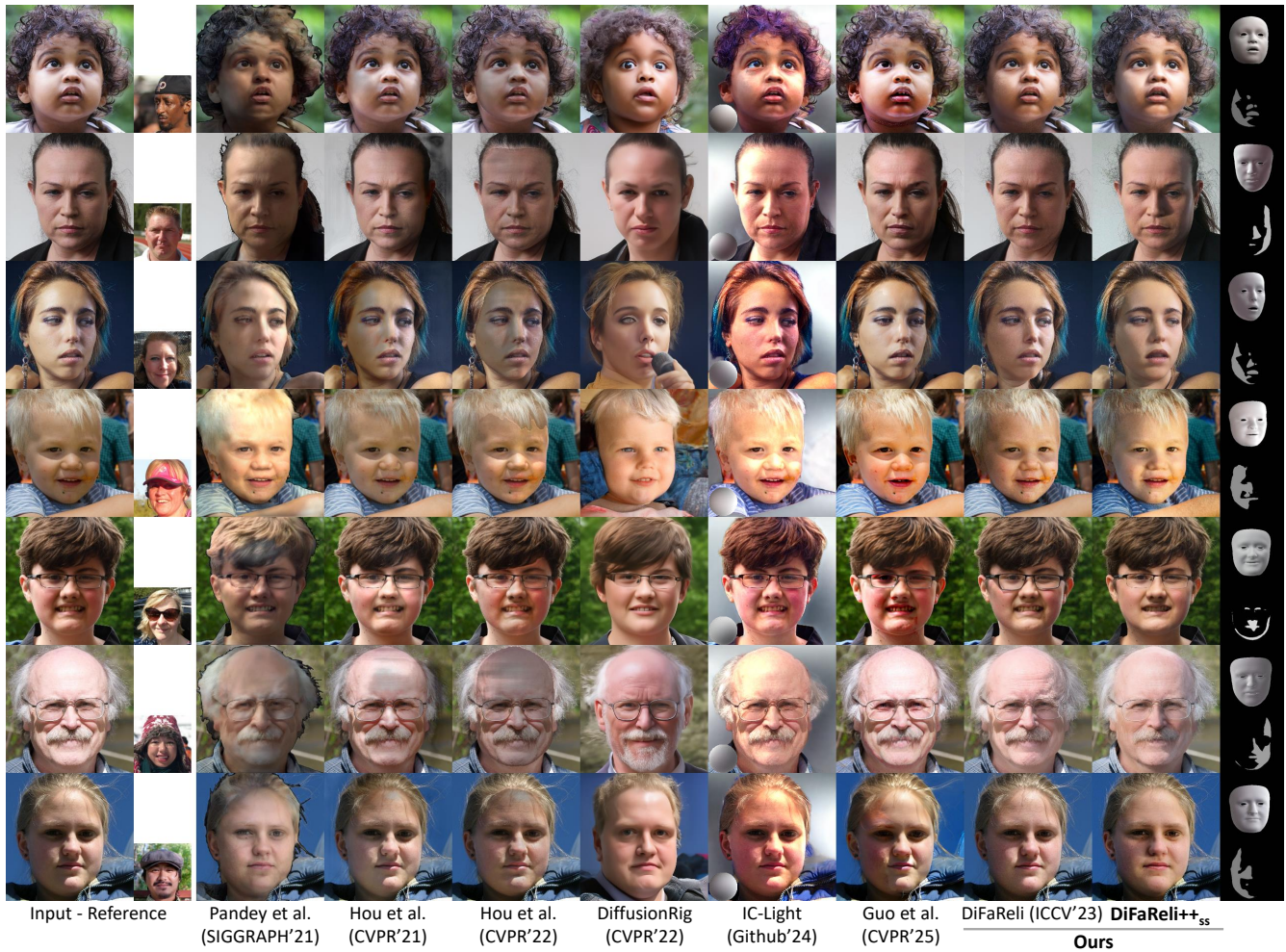


Fig. 32: Relit results under a given target lighting image on the FFHQ test set [32].

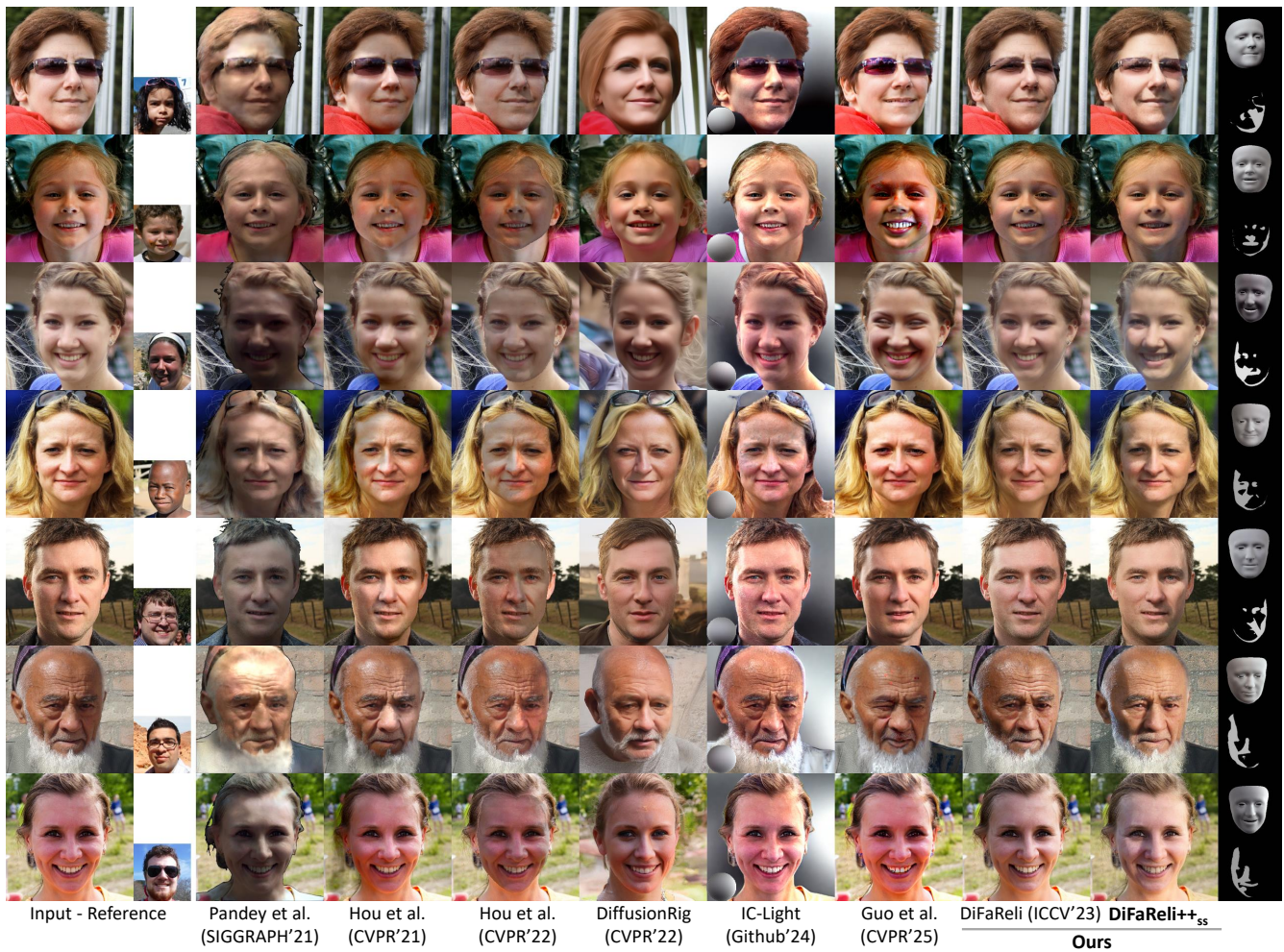


Fig. 33: Relit results under a given target lighting image on the FFHQ test set [32].



Fig. 34: Relit results under rotating HDR environment maps on the FFHQ test set [32].



Fig. 35: Relit results under rotating HDR environment maps on the FFHQ test set [32].

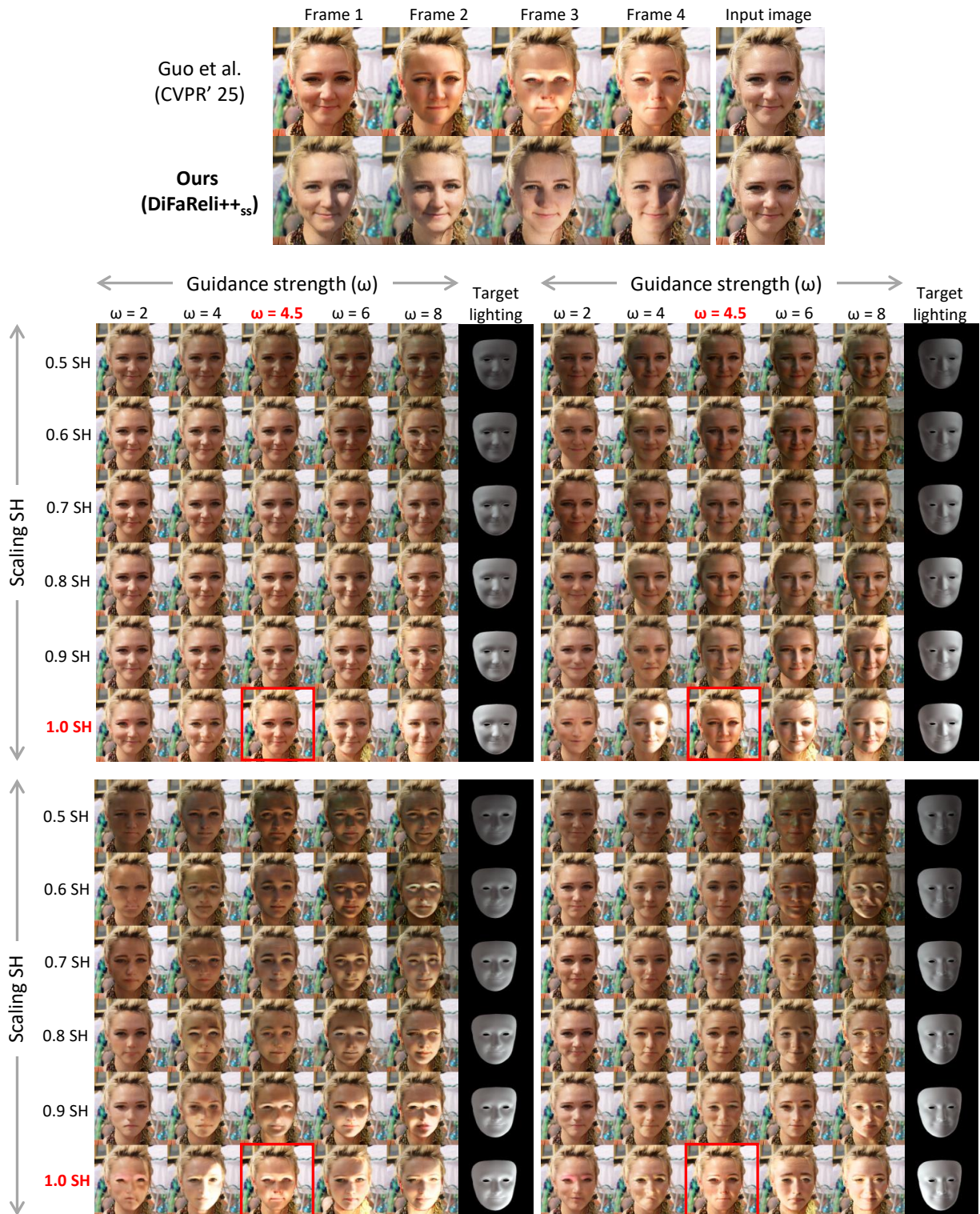


Fig. 36: **Tuning the relighting hyperparameters of Guo et al. [22] (under moving lights).** We performed a grid search over the guidance strengths (ω) proposed by [22] (see Table 5 in their supplementary material), along with scaling the SH values, to ensure that the oversaturation artifacts were not due to suboptimal hyperparameters. Results obtained with the default hyperparameters are highlighted with a red box.

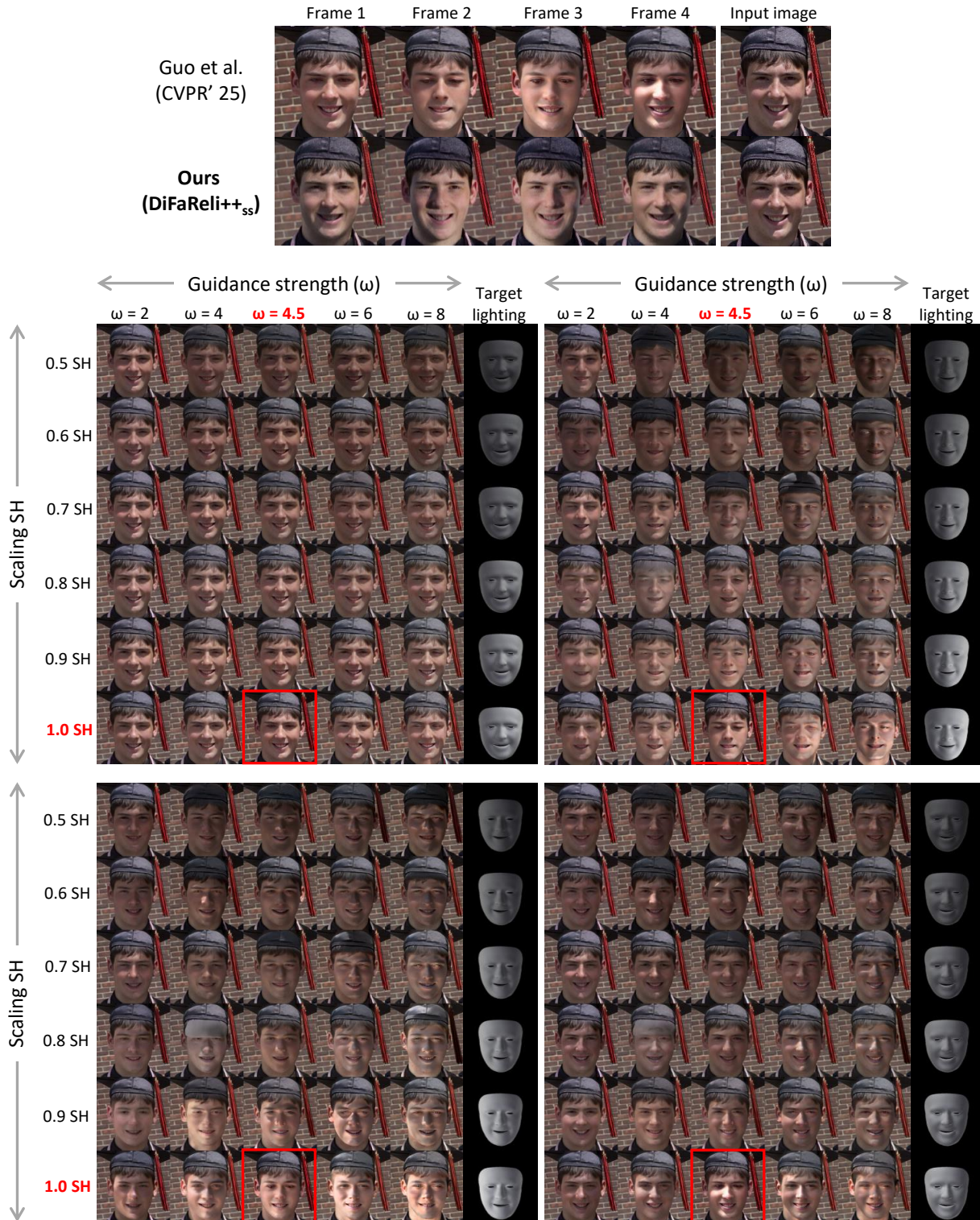


Fig. 37: **Tuning the relighting hyperparameters of Guo et al. [22] (under moving lights).** We performed a grid search over the guidance strengths (ω) proposed by [22] (see Table 5 in their supplementary material), along with scaling the SH values, to ensure that the oversaturation artifacts were not due to suboptimal hyperparameters. Results obtained with the default hyperparameters are highlighted with a red box.

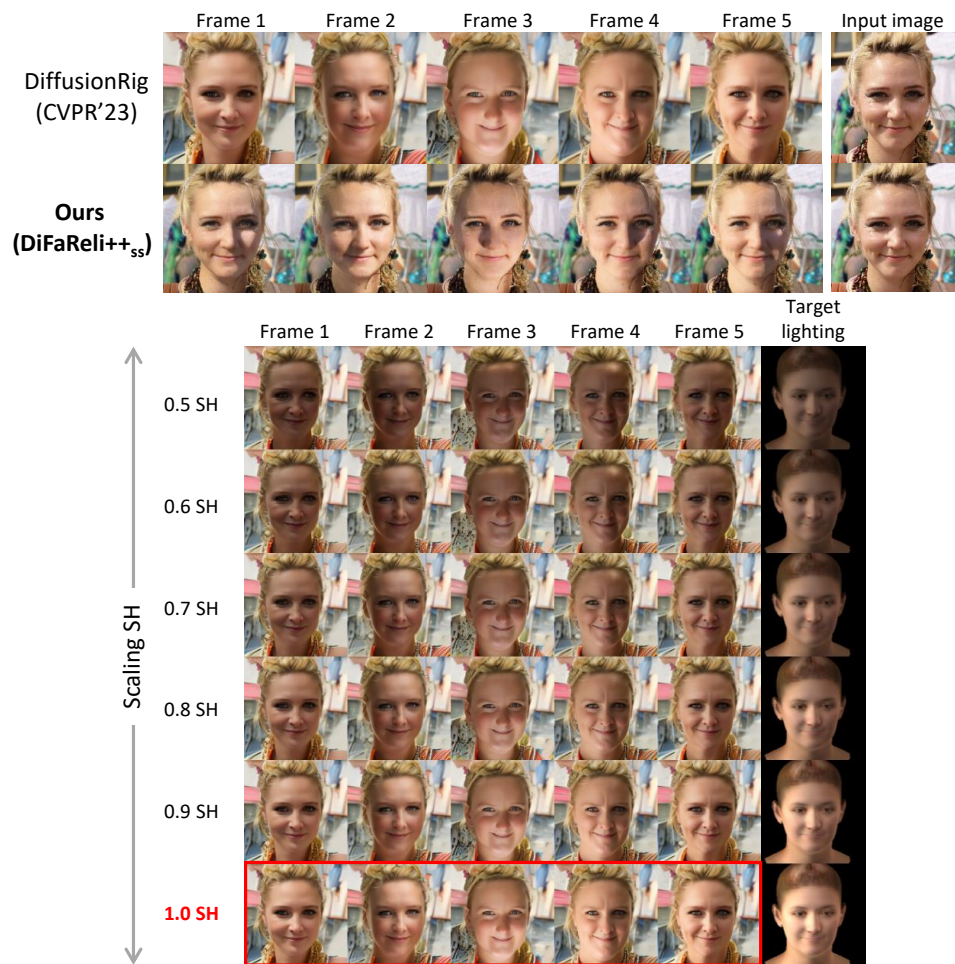


Fig. 38: **Tuning the relighting hyperparameters of DiffusionRig [13] (under moving lights)**. We performed a grid search over different scaled SH values to ensure that the oversaturation artifacts were not due to suboptimal tuning. Results obtained with the default parameters are highlighted with a red box.

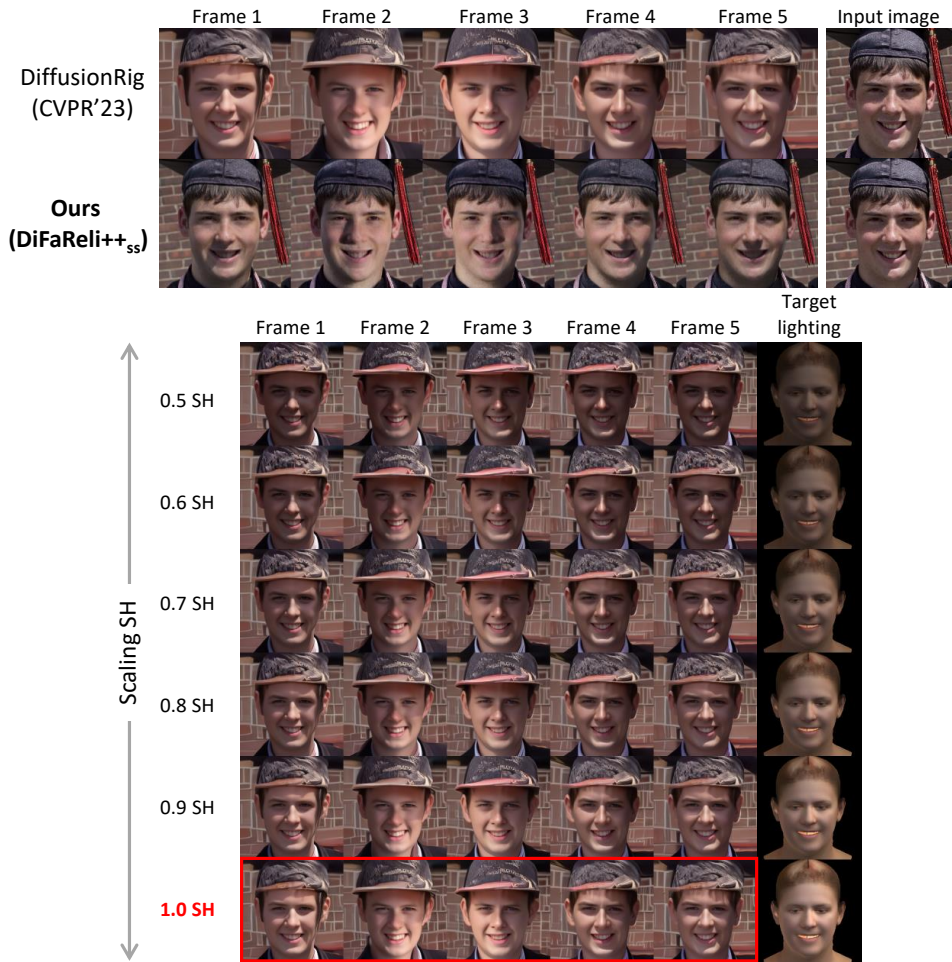


Fig. 39: **Tuning the relighting hyperparameters of DiffusionRig [13] (under moving lights)**. We applied the same relighting hyperparameter tuning procedure as described in Figure 38. Results obtained with the default parameters are highlighted with a red box

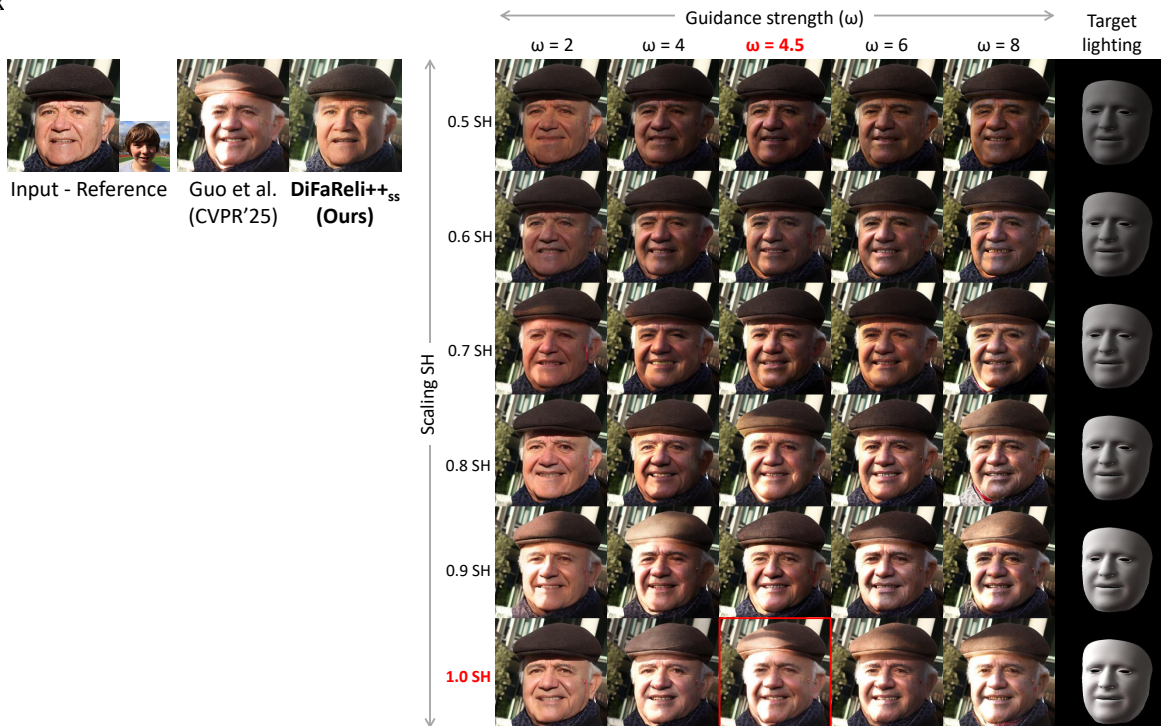


Fig. 40: **Tuning the relighting hyperparameters of Guo et al. [22] (under a target lighting image)**. We applied the same relighting hyperparameter tuning procedure as described in Figure 36. Results obtained with the default parameters reported in their paper is highlighted with a red box.

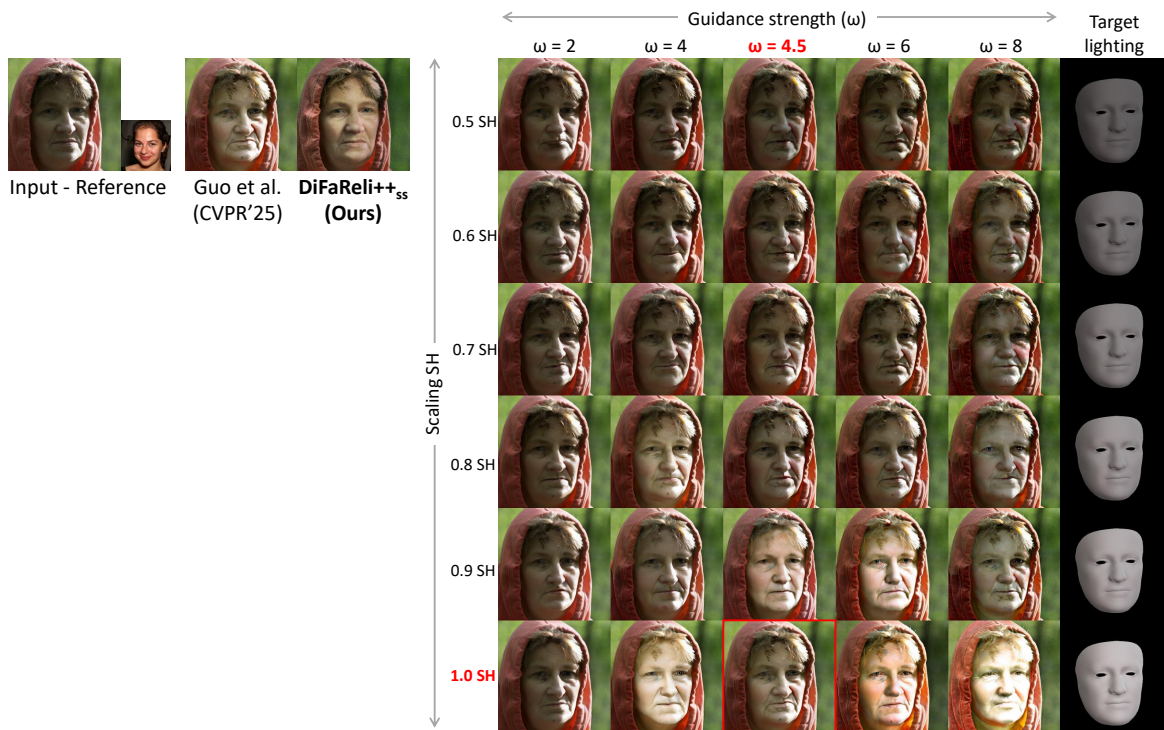


Fig. 41: **Tuning the relighting hyperparameters of Guo et al. [22] (under a target lighting image).** We applied the same relighting hyperparameter tuning procedure as described in Figure 36. Results obtained with the default parameters reported in their paper is highlighted with a red box.

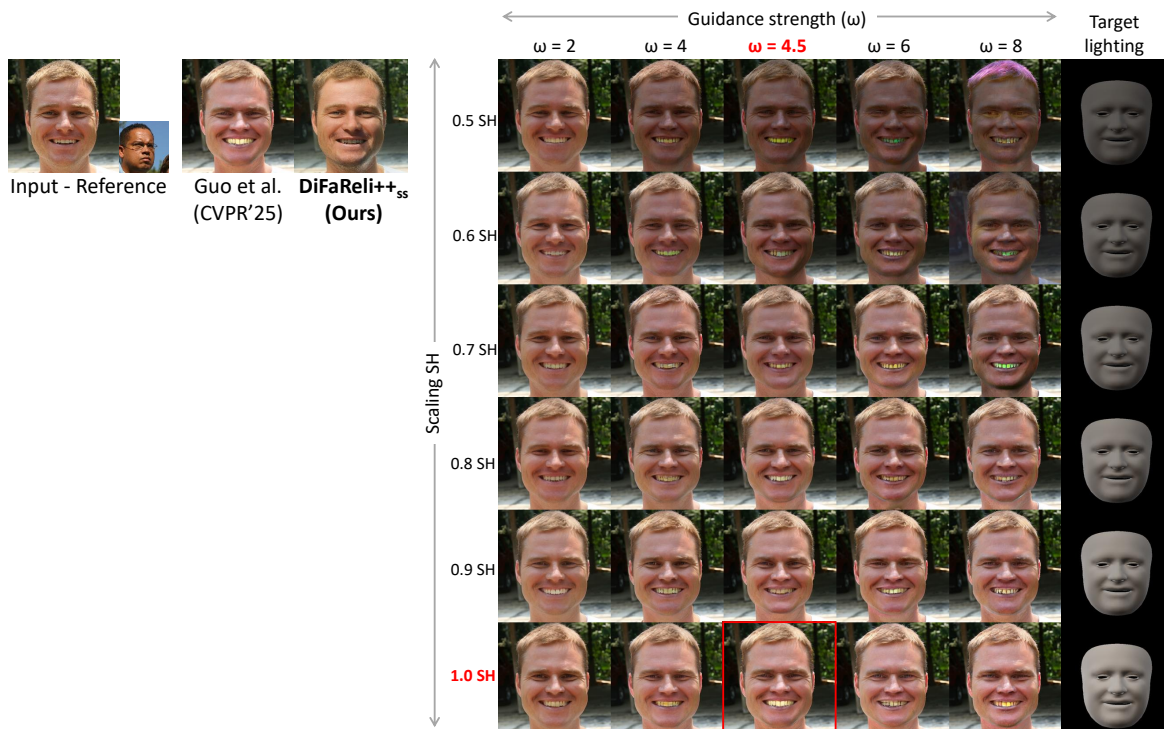


Fig. 42: **Tuning the relighting hyperparameters of Guo et al. [22] (under a target lighting image).** We applied the same relighting hyperparameter tuning procedure as described in Figure 36. Results obtained with the default parameters reported in their paper is highlighted with a red box.



Fig. 43: **Tuning the relighting hyperparameters of DiffusionRig [13] (under a target lighting image).** We applied the same relighting hyperparameter tuning procedure as described in Figure 38. Results obtained with the default parameters are highlighted with a red box.

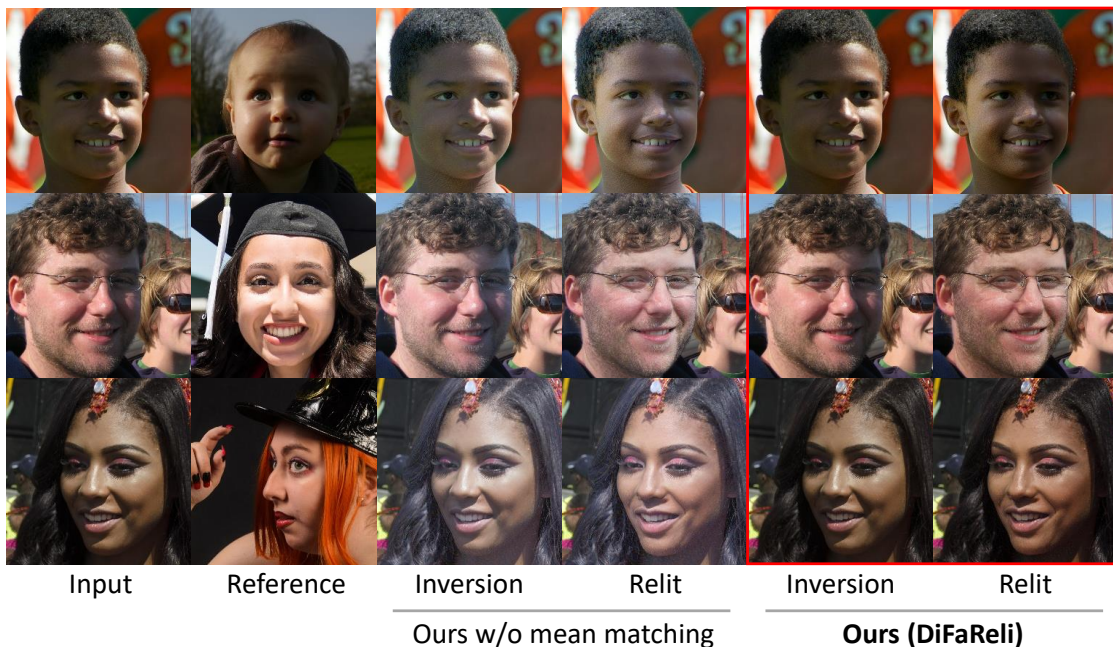


Fig. 44: **Improved DDIM sampling with mean-matching.** We show a qualitative comparison between “with” and “without” mean-matching. Our mean-matching technique helps correct the overall brightness in both the inversion output and relit image.



Fig. 45: Varying the intensities of cast shadows on FFHQ [32].

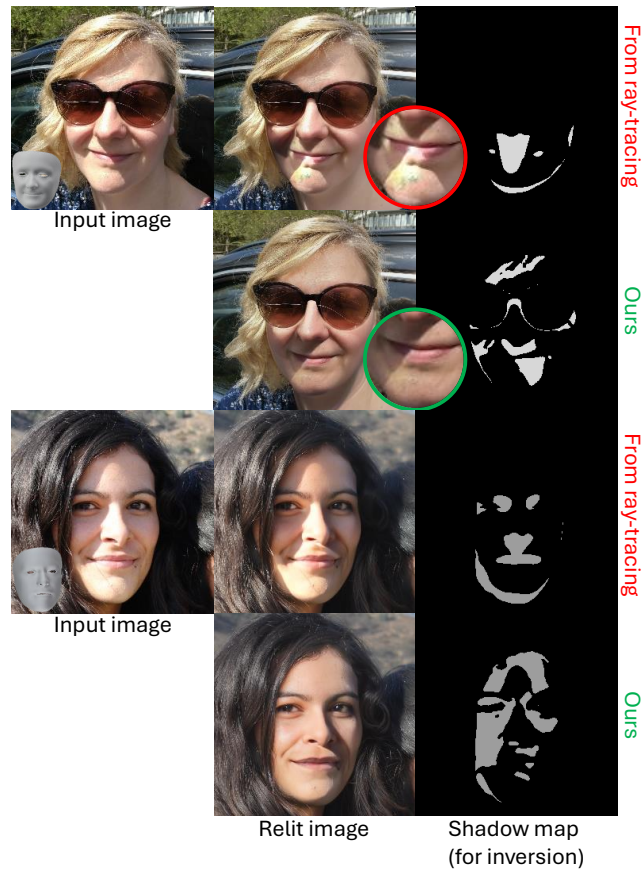


Fig. 46: **Poor results from using ray-traced shadow maps for inversion.** Using ray-traced shadow maps for DDIM inversion, the top result shows that non-shadow areas are over-brightened (highlighted with a red circle), while the bottom result shows a failure to remove shadows and closely follow the conditioning shadow map.

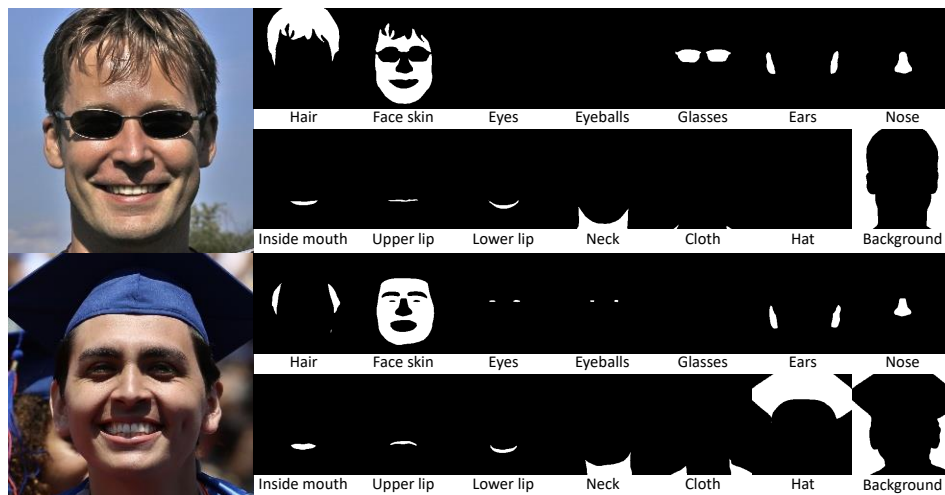


Fig. 47: **All segmentation masks** used as conditioning inputs in DiFaReli++ (Section IV-B in the main text).

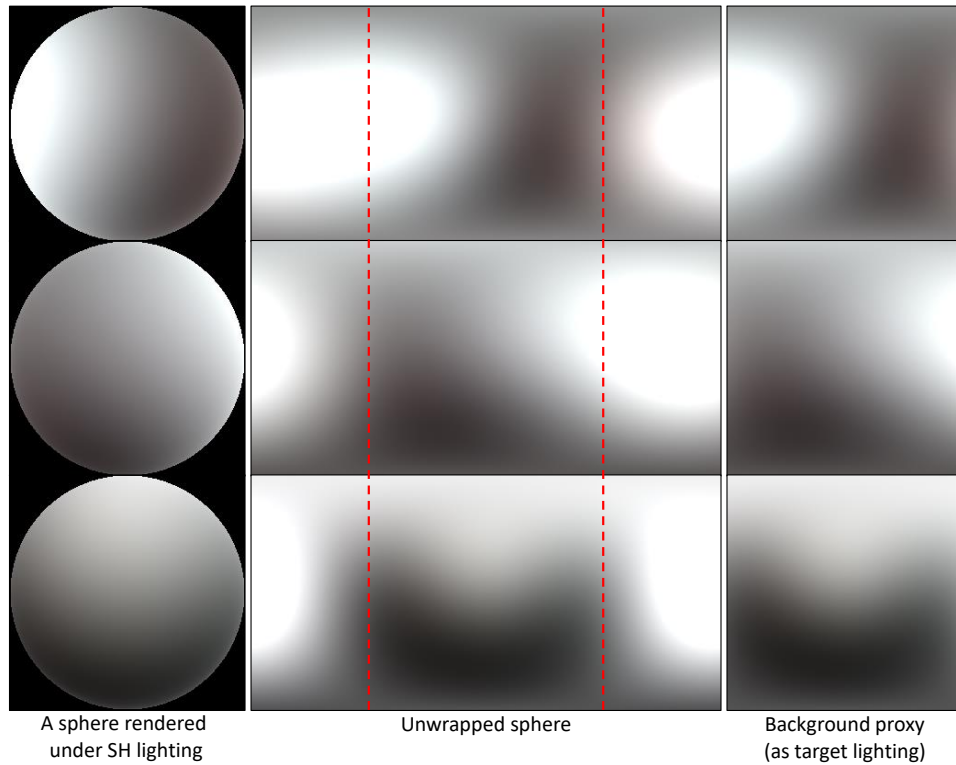


Fig. 48: Examples of proxy background images that serve as target lighting for IC-light [100].

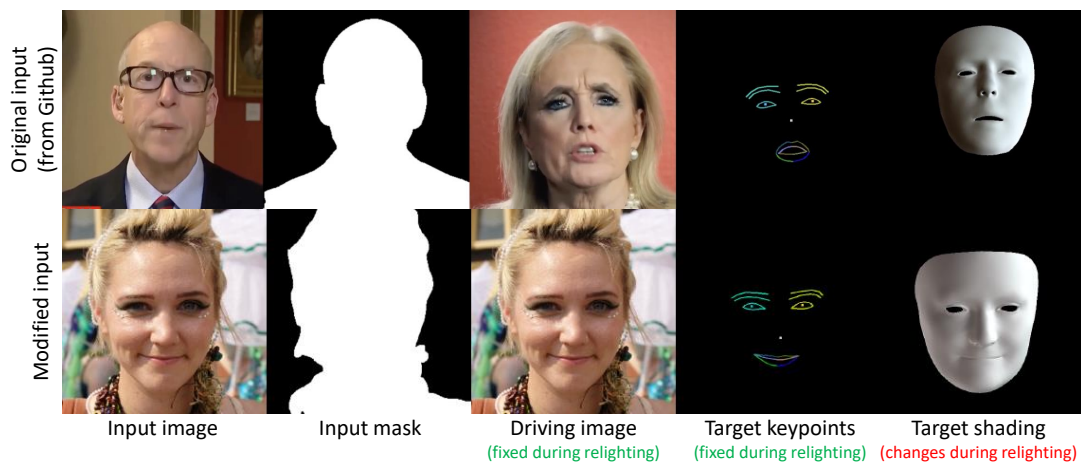


Fig. 49: **Example of original and modified inputs for [22].** We show the original inputs from the official GitHub repository of [22] (<https://github.com/MingtaoGuo/Relightable-Portrait-Animation>) and our modified versions adapted for the relighting task. In our modification, we fixed the driving image and target keypoints and changed only the target shading for relighting, thereby limiting control to relighting without animating the face.

Face Relighting Evaluation

This study has 10 tasks, each with 2 questions (20 total).

For each task, look at the input face image (A) and the target lighting, shown by another person and a diffuse ball under that lighting. Choose the result that makes the input person look naturally relit, with lighting and shadows consistent with the target lighting and with the input person's identity well preserved, based on:

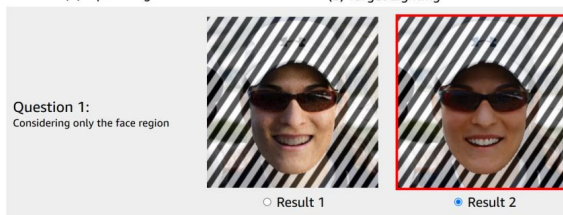
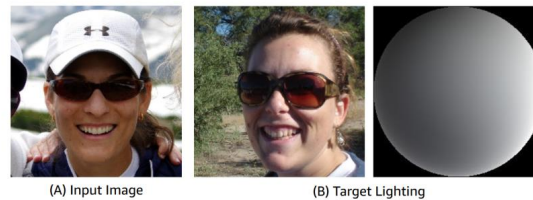
Criterion 1: Only the face.

Criterion 2: The entire person (face, hair, body, and clothing), *excluding the background*.

To answer: Click on the image or the radio button under it to select your choice. When finished with all questions, click 'Submit' at the bottom of this page.

Task 1

Which of these results most convincingly relights the input face image to match the target lighting?



Task 2

Which of these results most convincingly relights the input face image to match the target lighting?



Fig. 50: User interface for the relighting user study of facial and non-facial parts (Section V-C1 in the main text).

Face Relighting Evaluation

This study has 10 tasks, each with 2 questions (20 total).

For each question, look at the input face image (A) and the target lighting (B or C), shown as a video of a diffuse ball under the respective lighting. Then compare the results and choose the one that best matches the target lighting.


Choose the result that shows:

- Realistic relighting.
- Natural and consistent cast shadows that move correctly with the lighting.

To answer: Click on the video or the radio button under it to select your choice. When finished with all questions, click 'Submit' at the bottom of this page.


Task 1

Which of these results most convincingly relights the input face image and produces cast shadow effects based on the given target lighting?




(A) Input Image

Question 1:
Considering results relit with target lighting (B)



(B) Target Lighting




Result 1




Result 2


Question 2:
Considering results relit with target lighting (C)



(C) Target Lighting



Result 1



Result 2

Task 2

Which of these results most convincingly relights the input face image and produces cast shadow effects based on the given target lighting?



Fig. 51: **User interface for the relighting user study on relighting quality under moving lights** (Section V-C2 in the main text). In the interface, these results are videos that play simultaneously.

Face Relighting Evaluation

This study has 10 tasks, each with 2 questions (20 total).

For each question, look at the input face image (A) and the target lighting (B or C), which is shown as a video of a rotating environment map. This represents the surrounding light sources. As it rotates, you can see how the lighting would move around a face. Your task is to compare the two results and choose the one that best matches the target lighting.

Choose the result that shows:

- Realistic relighting.
- Natural and consistent cast shadows that move correctly with the lighting.

To answer: Click on the video or the radio button under it to select your choice. When finished with all questions, click 'Submit' at the bottom of this page.

Task 1

Which of these results most convincingly relights the input face image and produces cast shadow effects based on the given target lighting?



(A) Input Image

Question 1:
Considering results relit with *target lighting (B)*

(B) Target Lighting

Result 1

Result 2

Question 2:
Considering results relit with *target lighting (C)*

(C) Target Lighting

Result 1

Result 2

Task 2

Which of these results most convincingly relights the input face image and produces cast shadow effects based on the given target lighting?



(A) Input Image

Fig. 52: User interface for the relighting user study on relighting quality under rotating HDR environment maps (Section V-C3 in the main text). In the interface, these results are videos that play simultaneously.